Treatment of Glioblastoma tumors using photoactivated chemotherapy

Sina Katharina Goetzfried, Matthijs L. A. Hakkennes, Anja Busemann, Sylvestre Bonnet

Leiden Institute of Chemistry, Leiden University, Einsteinweg 55, 2333CC Leiden, The Netherlands

KEYWORDS

Photopharmacology, glioblastoma, cancer, neurotoxicity, photoactivated chemotherapy, ruthenium, metallodrugs

ABSTRACT: Glioblastoma multiforme (GBM) is highly aggressive, necessitating new therapies. Photoactivated chemotherapy (PACT) offers a promising approach by activating prodrugs with visible light at the tumor site. This study evaluated the anticancer activity of ruthenium-based PACT compounds in U-87MG glioblastoma cells and their safety in SH-SY5Y neuron-like cells. The compound [**3**]$(PF_6)_2$ showed promising light-activated anticancer effects in U-87MG cells, while [**1**]$(PF_6)_2$ was inactive, and [**2**]$(PF_6)_2$ was non-activated. Interestingly, in SH-SY5Y cells, light-activated [**3**]$(PF_6)_2$ increased cell proliferation, similar to Donepezil, without causing cell death. Increased Ca^{2+} uptake was observed, likely via interaction with the NMDA receptor, as suggested by docking studies. These findings suggest ruthenium-based PACT compounds as

potential treatments for GBM, effectively targeting cancer cells while preserving healthy neuronal cells.

Introduction

Albeit glioblastoma multiform (GBM) is one of the most common malignant primary brain tumors, its treatment continues to challenge the medical community today.[1,2] Each year, more than 250,000 new cases occur worldwide, while 200,000 patients die from this cancer with an annual growth rate of 1.5%.[3] According to recent studies, the incidence has increased from 0.73 to 4.49 per 100,000 people in the last 10 years worldwide.[4] Despite having a lower incidence compared to other cancers such as lung, breast or prostate cancer, GBM has a survival rate of 14-16 months and the five-year overall survival rate of less than 10%.[5] Novel therapeutically modalities are urgently needed.

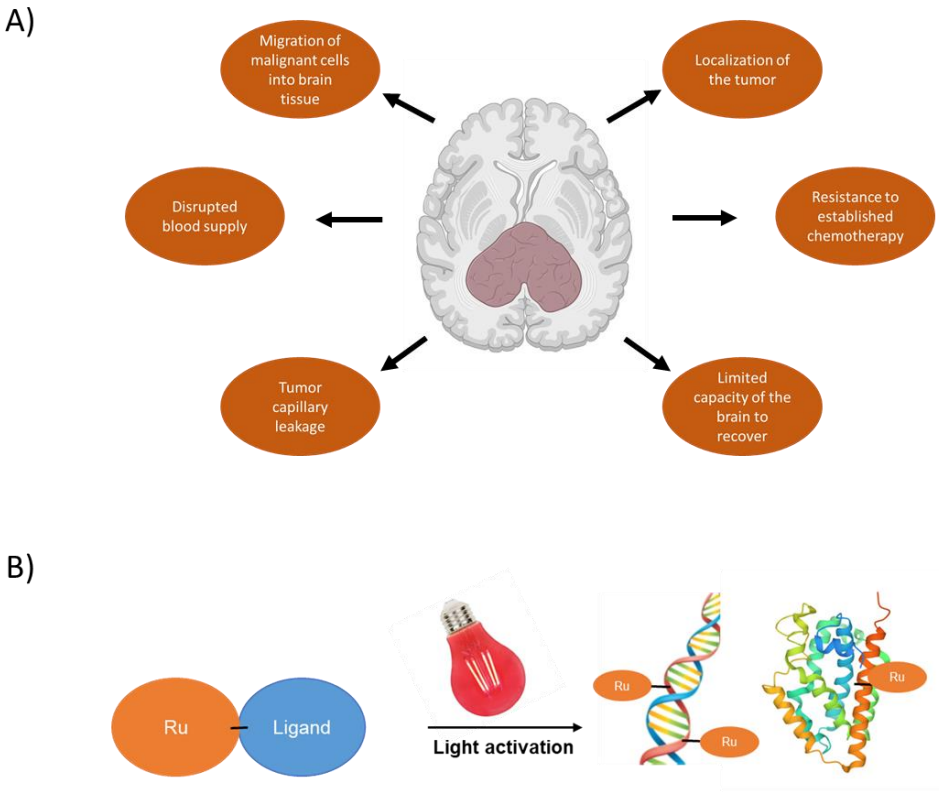

Figure 1. A) Schematic overview of the challenges in GBM treatment. B) Principle of ruthenium-based photoactivated chemotherapy (PACT).

Nowadays, treatment options are limited by the location, phenotype,[6,7] and aggressiveness of the tumor.[8] Figure 1A gives an schematic overview of the current problems in GBM treatment. Craniotomy, which consists in the surgical removal of the tumor, is still the first-line treatment, followed by radiation or chemotherapy.[9] Only a few chemotherapeutics received approval for the treatment of GBM, however:[10] lomustine,[11] intravenous carmustine, carmustine wafer implants,[12] temozolomide,[13] and the antibody bevacizumab.[14] The most challenging aspect of chemotherapy in GBM treatment is that many drugs cannot cross the blood-brain barrier (BBB), which prevents reaching tumours inside the brain and causes neurological side effects. This was notably observed for bortezomib, which failed in early clinical trials[15] or showed no significant improvements compared to current treatment methods.[15,16] Another issue is the heterogeneity of brain tumors, which leads to very different responses of GBM cells to most know drugs, including resistances.[17–19] Despite past drug development efforts, recurrence post-surgery are almost systematic, and patients suffer during treatment from severe side effects including nausea, vomiting, seizures and troubles with speech or memory.[20–24]

5-aminolevulinic acid (5-ALA) is a new agents that recently brought some light at the end of the tunnel.[25] It is a small molecule that does cross the BBB in high-grade GBM tumours. It then accumulates in malignant tissue, where it is converted into protoporphyrin IX (PPIX), a naturally occurring porphyrin that shows strong luminescence properties. This molecule can be used for fluorescence-guided surgery in GBM resection.[26–28] 5-ALA also opened the door to light therapy for brain tumor treatment.[29–31] PPIX has indeed excellent properties as photosensitizer for photodynamic therapy (PDT). PDT drugs are photocatalysts that convert under the action of visible light dioxygen to singlet oxygen ($^1O_2$) and other reactive oxygen species (ROS).[32,33] PPIX has shown very promising clinical results in non-resectable and in post-resection GBM treatment.[34,35]

On the other hand, PDT agents are known to cause necrosis in the surrounding area and are limited by the need for high oxygen concentrations.

Photoactivated chemotherapy (PACT), another recently developed phototherapeutic modality, may overcome these problems. PACT drugs are "photocaged" compounds consisting of two different components fused into a single prodrug that is biologically inactive. After exposure to light, the two molecules split, thereby recovering their anticancer properties. This method raises interest as it should lower side effects for patient like in PDT, but also protect the underlying healthy tissues from necrosis, which is often observed in clinical PDT. Ru^{2+}- or Pt^{4+}-based PACT compounds are the most developed PACT agents because the photochemistry of these two metal centers allows a coordination bond to be selectively broken, either by photosubstitution for Ru^{2+}, or by photoreduction for Pt^{4+}.[14] Typically, photochemical bond cleavage generates free organic inhibitors; however, the Ru-containing photoproduct can also generates phototoxicity by interacting with various biological targets (Figure 1B).[36,37] The photosubstitution mechanism involves thermal promotion from the excited metal-to-ligand charge transfer excited state (^{3}MLCT) generated photochemically, to a dissociative, low-lying triple metal-center state (^{3}MC), leading to elongation of a bond and further dissociation of the ligand, without changing the oxidation state of the metal center.[38,39]

Over the last decades, different ruthenium-based PACT compounds have been proposed for the treatment of different kind of tumors.[40–48] The use of ruthenium-based compounds to treat GBMs has rarely been reported.[49–51] Although in PACT the Ru polypyridine compounds used as photocages have often been reported as biologically inactive,[47,52] it should also not be ignored that drugs may be toxic to brain tissues adjacent to the targeted tumor, and therefore may cause neurotoxicity or excitotoxicity in an undesirable manner. Heavy metal elements often have a bad

reputation for their effects on health, but in fact little data is available on the pharmacology and toxicity of ruthenium polypyridyl complexes on the brain.

Here, we aimed to fill this knowledge gap by investigating *in vitro* if ruthenium-based PACT compounds may cause potential neuro- or excitotoxic effects that might limit their use for glioblastoma treatment. For this purpose, a series of known ruthenium-based PACT complexes with the general formula $[Ru(tpy)(N^N)(Hmte)](PF_6)_2$ (tpy: 2,2';6',2''-terpyridine; Hmte = 2-methylthioethanol; and N^N = bpy = 2,2'-bipyridine in [**1**]$(PF_6)_2$), N^N = i-biq = bisisoquinoline in [**2**]$(PF_6)_2$), N^N = i-diqa = di(isoquinolin-3-yl)amine in [**3**]$(PF_6)_2$), see Scheme 1),[53] were re-investigated *in vitro* in cell lines relevant for glioblastoma. We focused our study on two questions: on the one hand, the impact of these complexes on cancer cell proliferation using the classical GBM cell line U-87MG but also the neuronal-like, "healthy" cell line SH-SY5Y. On the other hand, we aimed to study the effects of these compounds, either in the dark or upon green light irradiation, on the intracellular Ca^{2+} level in the healthy SH-SY5Y cells, which may point to neuro- or excitotoxic effects. To ensure that the biological response is triggered exclusively by the ruthenium-based activated product, we used here complexes that photosubstitute a biological inactive ligand (Hmte).[53] Overall, the biological experiments proposed in this study represent a first methodological step towards more complete *in vivo* safety evaluation of the potential side effects of GBM treatment using ruthenium-based PACT.

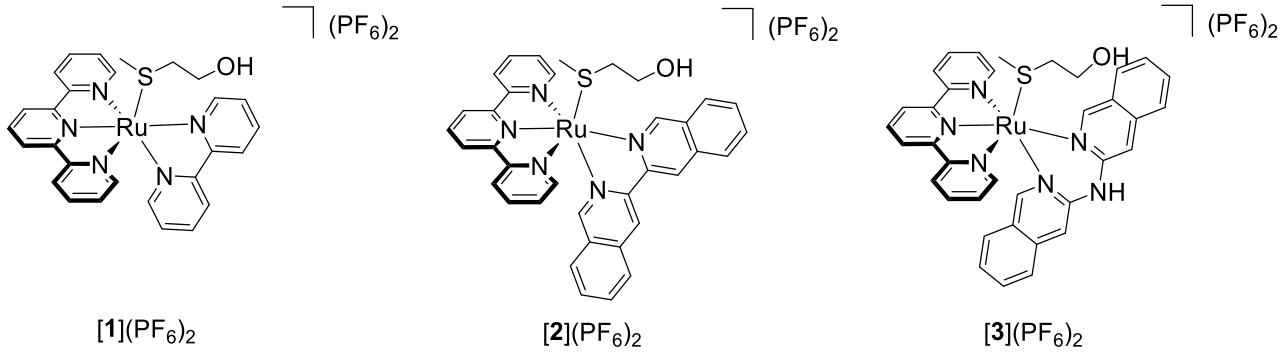

Scheme 1. Chemical structure of the complexes [**1**](PF$_6$)$_2$ -[**3**](PF$_6$)$_2$ used in this study.

Results

Cytotoxicity and cellular uptake in GBM cell line. With the aim to investigate the impact of ruthenium PACT compound on GBM cells, the compounds [**1**](PF$_6$)$_2$-[**3**](PF$_6$)$_2$ (Scheme 1) were incubated in U-87MG glioblastoma cells for 24 h at various concentrations, irradiated or not with green light (520 nm, 30 min, 25.2 J/cm^2) without exchanging the medium, and further incubated for 48 h, before measuring relative cell proliferation using a sulforhodamine B (SRB) end-point assay.[54,55] [**1**](PF$_6$)$_2$ did not show any cytotoxic effect (Table 1, Figure S1), which fits with earlier reports about the non-toxic character of [Ru(tpy)(bpy)(OH$_2$)]$^{2+}$ ([**4**]H$_2$O) in A375 skin melanoma or A549 lung cancer cell lines.[47,52,53] However, increasing the aromatic surface of the complex and therefore the lipophilicity of the prodrug resulted in anti-proliferative activity after light irradiation for [**2**](PF$_6$)$_2$ and [**3**](PF$_6$)$_2$ (Table 1, Figure S1). For [**2**](PF$_6$)$_2$ no significant difference was observed between dark and green light-activated conditions ($EC_{50,D}$ = 19 µM, $EC_{50,GL}$ = 23 µM, PI = 0.8). The most efficient PACT complexes was i-diqa bearing complex [**3**](PF$_6$)$_2$ which showed a photoindex of 3.5 ($EC_{50,D}$ = 37 µM, $EC_{50,GL}$ = 11 µM). Its noteworthy that our compounds were more efficient compared to the FDA approved compound Temozolomide, that is currently first-line treatment for GBM.

Table 1. Cytoxicity (EC_{50} in µM) of [**1**]$(PF_6)_2$-[**3**]$(PF_6)_2$ in glioblastoma U-87MG cells after kept in dark or after green light irradiation (520 nm, 30 min, 25.2 J/cm^2). [a]

Compound	$EC_{50,D}$ [µM]	CI_{95} [µM]	$EC_{50,GL}$ [µM]	CI_{95} [µM]	PI
[1](PF$_6$)$_2$	>100		61.66		>1.6
[2](PF$_6$)$_2$	19.4	+ 32.8 -14.4	23.3	+ 11.5 -8.5	0.8
[3](PF$_6$)$_2$	37.0	+8.2 -7.1	11.1	+4.4 -3.4	3.4
Donezepil HCl	>100		>100		
Temozolimde[a]	>100		>100		

[a]The cytotoxic experiments were performed in normoxic conditions (21% O_2) in biological and technical triplicates; errors indicate 95% confidence intervals (CI) in µM.[a] determined by MTT (3 mg/mL).

The cellular accumulation of Ru^{2+} can provide additional information about how differences in anticancer efficacy may relate to the amount of Ru prodrug in the cell before light activation. For instance, low uptake often leads to limited cytotoxicity due to limited access to the drug target. Therefore, we incubated [**1**]$(PF_6)_2$-[**3**]$(PF_6)_2$ (10 µM) in U-87MG cells during 6 or 24 h, and then quantified the intracellular Ru content using inductively-coupled plasma mass spectrometry (ICP-MS). Figure 2A display the metal content in ng Ru per millions cells. After 6 h 4-times lower amounts of [**1**]$(PF_6)_2$ (0.6 ng Ru/mio. cells) and [**2**]$(PF_6)_2$ (0.5 ng (Ru)/mio. cells) had been taken up compared with that measured for [**3**]$(PF_6)_2$ (2.1 ng (Ru)/mio. cells, Table S1). These numbers did not change significantly after 24 h incubation a slightly lower amount of [Ru] was found for [**1**]$(PF_6)_2$ (0.42 ng (Ru)/ mio. cells) [**3**]$(PF_6)_2$ (1.98 ng (Ru)/mio. cells). In terms of efficacy, the overall uptake was of only 0.5% for [**1**]$(PF_6)_2$ and 0.8 or 1.5% for [**2**]$(PF_6)_2$, while almost 11.4 or 11.5% of [**3**]$(PF_6)_2$ was taken up in U-87MG cells in such conditions. Similar results have been observed in A549 lung cancer cells previously.[53] It is surprising to find such different uptake values for [**2**]$(PF_6)_2$ and [**3**]$(PF_6)_2$, as both compounds have similar LogP values (3.08 and 2.92,

respectively).[53] For unknown reasons it appears that the amine bridge in the i-diqa ligand facilitates uptake of the ruthenium compound [**3**](PF$_6$)$_2$.

To further investigate in which compartment in the cells the ruthenium complexes localized before light activation, we used a FractionPrep cell fractionating kit to separate the different compartments (cytosol, membrane, nucleus and cytoskeleton) of the cells, and analysed Ru content of all fractions by ICP-MS for U-87MG cells treated for 24 h with 10 µM [**2**](PF$_6$)$_2$ or [**3**](PF$_6$)$_2$ (

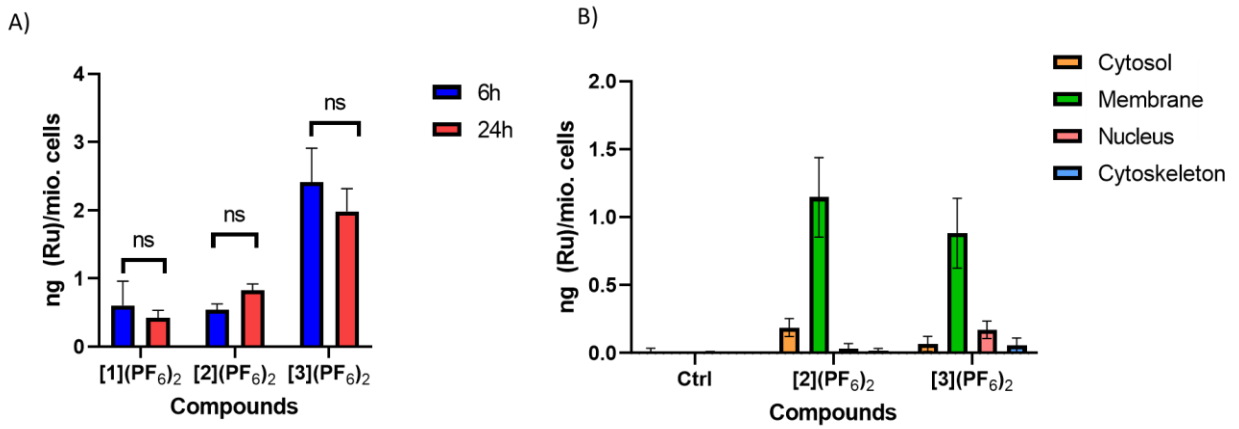

Figure 2B and Table S2). [**1**](PF$_6$)$_2$ was excluded from this experiment as it was poorly cytotoxicity and showed a very low uptake in previous experiments. As depicted in Figure 2B, both [**2**](PF$_6$)$_2$ and [**3**](PF$_6$)$_2$ were mostly found in the membrane fraction (0.83 or 0.88 ng Ru/ mio. cells). Small amount of [**2**](PF$_6$)$_2$ were found in the cytosol (0.18 ng Ru/ mio. cells) while almost the same amount (0.17 ng Ru/ mio. cells) was recorded for [**3**](PF$_6$)$_2$ in the nucleus. Almost no Ru was detected in the cytoskeleton for both complexes. As note, those data only provides information where the prodrug was localized before light activation, but it does not say anything on where the activated photoproducts go.

Within this series of structurally related compounds, several trends can be highlighted. First, [**1**]$(PF_6)_2$ was poorly phototoxic due to very low cellular uptake. Surprisingly, the exchange of the bpy ligand by i-biq increased cytotoxicity at least by a 3-fold factor, although uptake did not increase significantly; still, no difference between dark and light EC_{50} values were seen for this complex in this GBmM cell line. The best light-activated figure-of-merit in this series was observed for [**3**]$(PF_6)_2$. This complex became 3.5 times more toxic upon green light irradiation compared with dark conditions; compared with [**2**]$(PF_6)_2$, it was twice less cytotoxic in the dark in spite of the 4 times higher uptake, and twice more cytotoxic after light irradiation. In addition, the uptake and fractionation results are compatible with a membrane association of both active complexes, and a poor cellular uptake before activation. As a note, it is impossible to image and co-localize ruthenium-based PACT complexes in a cell by confocal microscopy as these compounds are non-emissive.

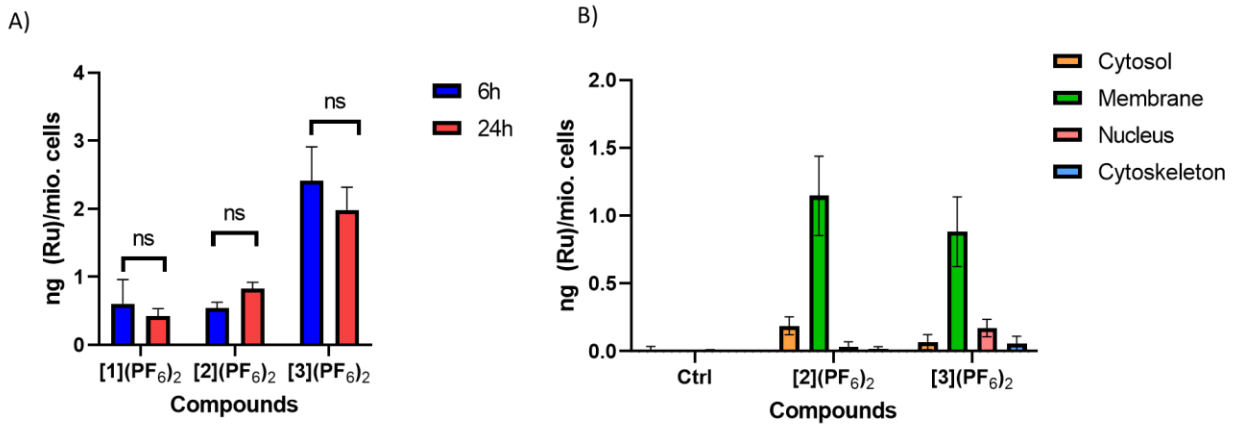

Figure 2. *(A)* Total Ru cellular uptake in U-87MG cells after 6 (blue bars) and 24 h (red bars) incubation time in the dark. *(B)* Ru content of different cell fraction*s* after 24 h incubation time. Ru concentrations: 10 µM.

In vitro approach to neurotoxicity. With these results in hand, we wondered how to investigate *in vitro* the potential neurotoxicity of these compounds, hence their damaging properties towards adjacent, healthy neurons. Testing the neurodamaging effects of chemical compounds is a difficult venture as it comes in hand with unique difficulties.[56–59] Several *in vivo* characteristics, e.g. the low neurogenesis in adults; a great level of cellular, structural, and chemical heterogeneity; distinct metabolic requirements; and the large number of neuronal messengers, renders the nervous system particularly vulnerable to damages induced by chemicals. When used for treating brain tumors, new chemotherapy compounds, even photoactivated ones, may potentially impair sensory and motor functions or interfere with the memory process, for example, which is difficult to test *in vitro*. However, some tests have been proposed, including the inhibition of different enzymes such as acetylcholine esterase (AChE), the GABA receptors, the *N*-methyl-*D*-aspartate (NMDA) receptors, or the serotonin receptors. Last but not least, the neuroblastoma cell line SH-SY5Y has been proposed as a suitable cell line to evaluate the neuro- and excitotoxic effects of chemical compounds, usually not in cancer research but for developing drugs against neurodegenerative diseases.[60–64]

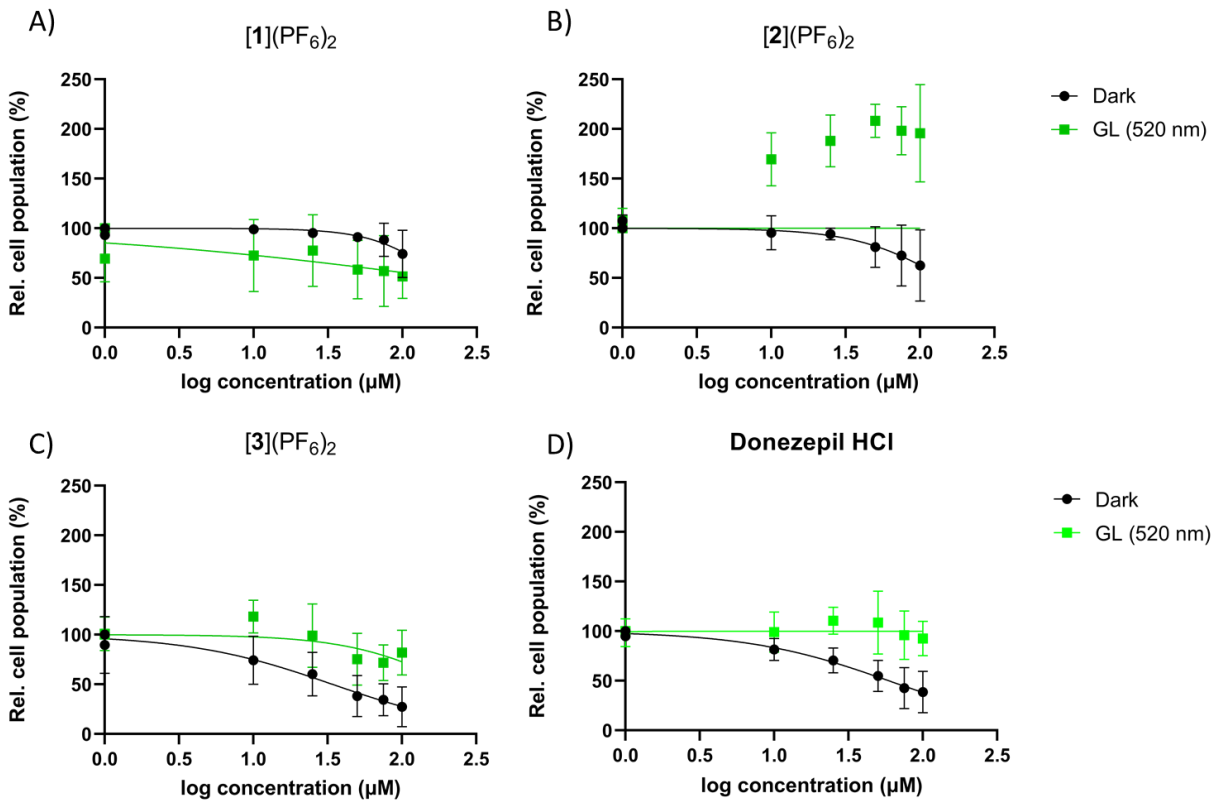

Figure 3. Dose-response curve of [**1**]-[**3**](PF$_6$)$_2$ complexes and Donepezil HCl in SH-SY5Y cells in the dark and upon green light activation (30 min, 520 nm, 25.2 J/cm^2). Cells were irradiated with green light 24 h after compound administration.

Using the same protocol as for the U-87MG cancer cell line, we first investigated the cytotoxicity of [**1**](PF$_6$)$_2$-[**3**](PF$_6$)$_2$ in the sympathetic ganglion neurons-like SH-SY5Y cell line. The HCl salt of the acetylcholine esterase inhibitor Donepezil, Donepezil HCl, was included in the study as typical, clinically approved drug used for treating brain diseases such as Alzheimer's disease.[65] The cells were hence were incubated with increasing concentrations of each compounds 24 h in the dark, irradiated with light without changing the medium, and further incubated 48 h before the end point SRB assay (Figure 3, Table 2).[54,55] In the dark, [**1**](PF$_6$)$_2$, and [**2**](PF$_6$)$_2$ required high concentrations (> 40 µM) to block cell growth. Only [**3**](PF$_6$)$_2$ possessed EC$_{50}$ values below 50 µM. Unexpectedly, when the ruthenium compounds were exposed to green light (520 nm, 30 min,

25.2 J/cm^2), a reverse effect was observed compared with U-87MG cells: more protein was observed in the SRB assay than in the dark, suggesting an increased number of living cells at t=96 h time point, up to 200% for [**2**](PF$_6$)$_2$ (Figure 3B). For [**3**](PF$_6$)$_2$ the end-point relative cell population remained close to 100%, suggesting that the limited toxicity observed in the dark had been completely cancelled (Figure 3C). It is also worth noticing that green light alone had an impact on the growth of SH-SY5Y cells, as cells irradiated with light in absence of Ru compound showed reduced cell growth by ~50% compared with cells kept in the dark. The ruthenium prodrugs seem hence to protect the cells against this effect. Our results in absence of compound confirmed previous studies on SH-SY5Y cells that had shown that green light irradiation influenced dendrite elongation and reduced cell growth.[66] These observations were, surprisingly, similar to that of Donepezil HCl (Figure 3D), which slightly reduced the proliferation of SH-SY5Y cells in the dark (EC_{50} = 59 µM) but had no impact on cell growth after the cells had also been irradiated with green light.

Table 2. Cytotoxicity (EC_{50} with 95% confidence interval (CI), in µM) of [**1**](PF$_6$)$_2$-[**3**](PF$_6$)$_2$ in SH-SY5Y cells either kept in dark or following green light irradiation (520 nm, 30 min, 25.2 J/cm^2).[a]

Compound	$EC_{50,D}$ [µM]	CI_{95} [µM]	$EC_{50,GL}$ [µM]	CI_{95} [µM]	PI
[1](PF$_6$)$_2$	>100	-	>100	-	-
[2](PF$_6$)$_2$	>100	-	>100		-
[3](PF$_6$)$_2$	34.2	+16.8 -12.05	>100		-
Donepezil HCl	59.1	+31.0 -16.6	>100		

[a]The cytotoxic experiments were performed under normoxic conditions (21% O_2) in biological and technical triplicates; errors indicate 95% confidence intervals (CI) in µM.

These surprising results led us to further investigate whether the uptake of the respective compounds plays a pivotal role in the alternation of the proliferation. First, we checked the ruthenium content of the most potent compound [**3**]$(PF_6)_2$ (10 μM) in SH-SY5Y cells when cells were kept in the dark or irradiated with green light (520 nm, 30 min, 25.2 J/cm^2). Therefore, we incubated SH-SY5Y cells with the complex but instead of 24 h dark incubation time, we irradiated 6 h after compound addition, as previous studies on the U-87 MG cell line did not show any significant difference in the Ru-uptake level at 6 or 24 h incubation time. The complex was allowed to incubate for 24 h after irradiation, before the ruthenium cellular content was analysed by ICP-MS. As Figure 4A and Table S3 illustrates, a seven times higher Ru content was found after [**3**]$(PF_6)_2$ had been activated with green light (15.5 ng (Ru)/ mio cells) compared to unactivated complex (2.4 ng (Ru)/ mio. cells) that is almost equal to that found in U-87MG cells. Like in U-87MG cancer cells, [**1**]$(PF_6)_2$ (dark: 0.4 ng (Ru)/ mio. cells; GL: 0.9 ng (Ru)/ mio. cells) and [**2**]$(PF_6)_2$ (dark: 1.0 ng (Ru)/ mio. cells; GL: 3.2 ng (Ru)/ mio. cells) were poorly taken up even when twice the concentration (20 μM) was administered compared to [**3**]$(PF_6)_2$. We finally decided to incubate the SH-SY5Y cells with the EC_{50} values obtained from the cytotoxicity experiment using the U-87MG cell, as those procedure would allow to observe the effect of the prodrug on the healthy neuron-like cells when treated with the phototoxic compound dose. It is important to note that in all the complexes we tested, the light-activated species resulted in higher concentrations of ruthenium within cells, suggesting that the activated drug may accumulate more effectively than the prodrug (as already observed in A549 and A375 cancer cells). For [**1**]$(PF_6)_2$ and [**2**]$(PF_6)_2$ these higher ruthenium levels after activation did not lead to a lower cell population, though. Overall, cellular uptake in neuron-like SH-SY5Y cells followed the same trends as for GBM cells U-87MG in the dark, while uptake was much higher after light activation.

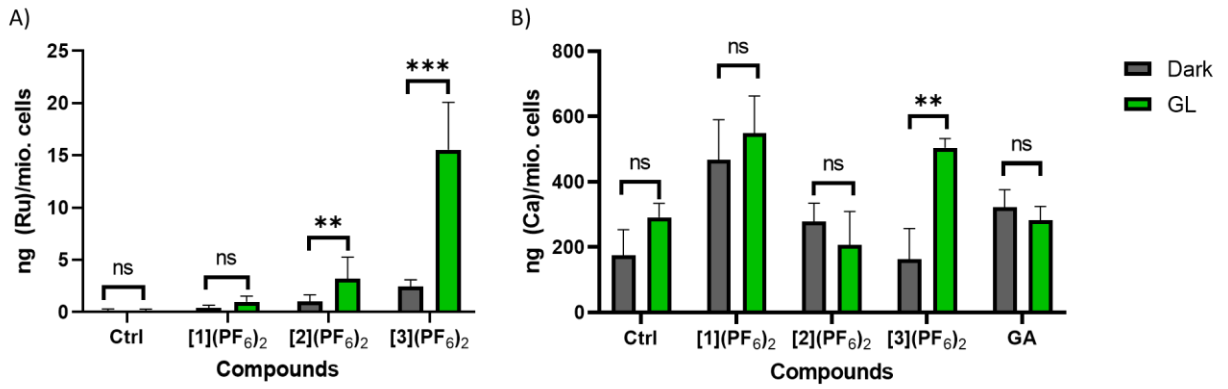

Figure 4. Ru (A) and Ca (B) content of SH-SY5Y cells treated with [**1**](PF$_6$)$_2$ and [**2**](PF$_6$)$_2$ (20 µM) and [**3**](PF$_6$)$_2$ (10 µM). 6 h after incubation times cells were irradiated with green light (520 nm, 30 min 25.2 J/cm^2) or kept in dark. Untreated cells served as negative control, while cells treated with L-glutamic acid (GA, 10 µM) were used as positive control for enhanced Ca uptake. After an overall 30 h incubation time, cells were collected and Ca and Ru content was recorded via ICP-MS.

Another indication of the neurological toxicity of chemicals can be obtained by measuring the intracellular level of calcium in healthy neurons. Ca^{2+} ions are important secondary messengers that regulate membrane excitability, dendrite development, and contribute in various primary neuronal functions such as neurotransmitter synthesis and release, neuronal excitability, information processing, and memory storage.[67] Dysregulation of intracellular Ca^{2+} ion concentration leads to neuronal cell death and brain damage, as demonstrated years ago in AD studies.[68–71] Brain aging is also characterized by changes in the calcium homeostasis.[72,73]

Thus, we investigated the impact of treatment with ruthenium complexes [**1**](PF$_6$)$_2$, [**2**](PF$_6$)$_2$ and [**3**](PF$_6$)$_2$ on the intracellular Ca^{2+} level of SH-SY5Y cells. 6 h after compound addition, cells were irradiated with green light or kept in dark. Intracellular Ca^{2+} levels were then assessed by ICP-MS 24 h after light activation. The NMDA and the α-amino-3-hydroxy-5-methyl-4-isoxazole propionic acid (AMPA) receptors being glutamate-gated cation channels that allow for an increase of calcium permeability of the neuron membrane, we also used glutamic acid (GA, 10 µM), a known NMDA and AMPA activator, as positive control in this assay. Glutamate showed twice higher Ca^{2+} levels (322 ng (Ca)/mio. cells) compared to vehicle control (175 ng (Ca)/mio. cells). As displayed in Figure 4B and Table S3, elevated Ca^{2+} levels were found for cells treated with [**1**](PF$_6$)$_2$ (467 ng (Ca)/mio. cells) and [**2**](PF$_6$)$_2$ (279 ng (Ca)/mio. cells) in the dark, compared to

untreated cells (175 ng (Ca)/ mio. cells), while for [**3**](PF$_6$)$_2$ almost the same amount of calcium was found as in untreated cells (163 ng (Ca)/ mio. cells). Strikingly, after light irradiation the intracellular Ca^{2+} content increased 3-fold for activated [**3**](PF$_6$)$_2$ (504 ng (Ca)/ mio. cells), while for [**1**](PF$_6$)$_2$ (549 ηg (Ca) /mio. cells) and [**2**](PF$_6$)$_2$ (325 ng (Ca)/ mio. cells) only a slightly increase of Ca^{2+} was found, compared to dark conditions. Notably, green light alone had a significant impact on intracellular Ca^{2+} accumulation, which raised 2-fold from 175 in the dark to 291 ng (Ca)/ mio. cells in untreated, light-irradiated cells. Notwithstanding, we did not observe any correlation between elevated Ca^{2+} levels and reduced cell proliferation or the presence of floating cells within treated wells.

Among all enzymes involved in trans-membrane-signaling, another important one is acetylcholinesterase (AChE). In a modified procedure (for further details see Experimental section) we checked whether the ruthenium complexes were able to inhibit AChE in the dark and after light-activation. The colorimetric assay used the Ellman's reagent. In short, [**1**](PF$_6$)$_2$, [**2**](PF$_6$)$_2$ and [**3**](PF$_6$)$_2$ were incubated at different concentrations with the isolated enzyme, and kept in the dark or irradiated with green light (520 nm, 30 min, 25.2 J/cm^2). The conversion of 5,5′-dithiobis-(2-nitrobenzoic acid) (DTNB) to the yellow 2-nitro-5-thiobenzoate (TNB) initiated by the addition of acetylthiocholine was then detected by UV-vis spectroscopy every 5 min for a total time of 40 min. Donepezil HCl, a known AChE inhibitor, was used as a positive control. Respective IC_{50} values were calculated from the inhibition values 40 min after DTNB addition (Table 3 and Figure S2, Supporting Information). In the dark, almost all compounds had an IC_{50} above the highest concentration (15 μM) used, except [**3**](PF$_6$)$_2$ which had an IC_{50} of 9.6 μM. Upon light irradiation, all compounds were able to inhibit ~50% of the enzyme activity. Nevertheless, no complex reached inhibitory effects comparable to that of Donepezil HCl which blocked AChE activity completely at the lowest concentration (1 μM). Overall, the ruthenium complexes seemed to weakly inhibit AchE in a light-dependent manner, but none of them were significant inhibitors notably compared to Donepezil HCl.

Table 3. AChE effective inhibitory concentrations (IC_{50} with 95% confidence interval in μM) of ruthenium compounds [**1**]-[**3**](PF$_6$)$_2$ in the dark and after green light irradiation (GL).

Compound	$IC_{50,D}$ [µM]	95% CI	$IC_{50,GL}$ [µM]	95% CI	PI
[1](PF$_6$)$_2$	>15		6.74	+0.96 -0.92	>2.2
[2](PF$_6$)$_2$	>15	-	10.29	+3.88 -2.10	>1.5
[3](PF$_6$)$_2$	9.60	+3.26 -1.96	5	+0.45 -0.44	2
Donepezil HCl	<1		<1		

Computational Study. Uptake of Ca^{2+} ions is regulated by a multitude of transport systems e.g. the direct NMDA and AMPA receptors, but also indirectly via serotonins receptors and calcium/calmodulin dependent protein kinase II and IV (CAMK2 and CAMK4). The substantial increase in intracellular Ca^{2+} levels after irradiation of [**3**](PF$_6$)$_2$ led us to wonder whether this metal complex may inhibit Ca^{2+} transporters. Having noticed a comparable trend in the cytotoxicity between [**3**](PF$_6$)$_2$ and Donepezil HCl on the U-87MG and SH-SY5Y cell lines, we decided to perform a docking study of Donepezil HCl to all the calcium receptor targets. In order to investigate this question, we performed a computational screening of the inhibitory properties of the ruthenium compound [**3**]$^{2+}$ and its light-activated aqua analogue [**4**]$^{2+}$ (see Scheme 2) towards different calcium transmembrane transport systems to identify their potential inhibitory targets.

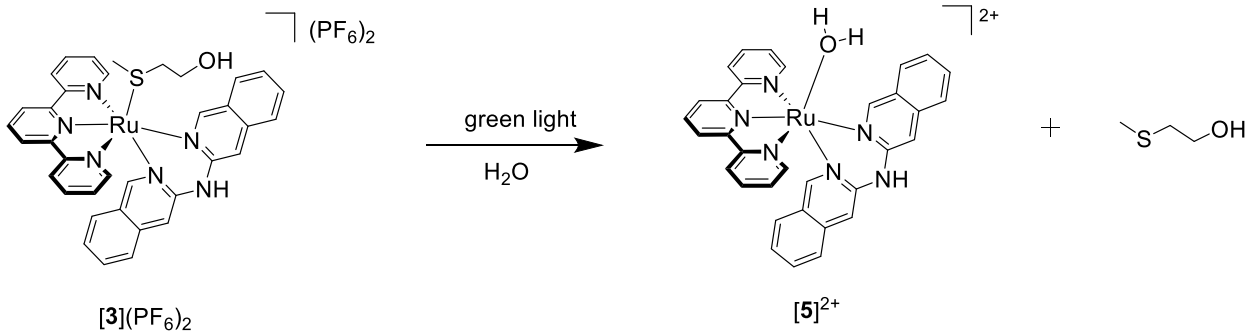

[**3**](PF$_6$)$_2$ [**5**]$^{2+}$

Scheme 2. Chemical structures used for docking studies with MetalDock. The aqua ligand of [**4**]$^{2+}$ was removed from the x,y,z coordinate file before docking.

Using the MetalDock docking program recently published by our group,[74] we investigated the interaction of the non-irradiated compound, $[\mathbf{3}]^{2+}$, where Hmte is still coordinated to ruthenium, and of the light-activated analogue, $[\mathbf{5}]^{2+}$, where Hmte is dissociated and there is hence an aqua ligand bound to ruthenium instead. After photosubstitution of Hmte by water, coordination of metal-binding residues of the different protein targets to ruthenium is possible, which usually renders docking studies impossible. Our MetalDock program, however, allows testing also such metal-based inhibitors. The water molecule of $[\mathbf{5}]^{2+}$ was hence removed, and both ruthenium complexes were docked with the NMDA (PDB: 7EOR), AMPA (PDB: 5YBG, 5ZG0, 4LZ5, 4LZ7), CAMK2 (PDB: 2VZ6), CAMK4 (PDB: 2VZ2), serotonin (7WC4, 7WC6) and AChE (PDB: 4EY7) receptors after removing the co-crystallized organic inhibitor usually present in published crystal structures. We used a 30 x 30 x 30 Å box centered around the original organic inhibitor bound to the protein X-ray structure in the PDB files. During each docking simulation ten poses were generated. Strikingly, the docking of $[\mathbf{3}]^{2+}$ and $[\mathbf{5}]^{2+}$ to the active site of the NMDA receptor resulted in poses that fitted very well in the binding pocket and showed clear-cut interactions with different residues. For $[\mathbf{3}]^{2+}$, four poses were obtained in which the Hmte ligand formed a hydrogen bond with the carboxylate of GLU-530, while four others showed the Hmte ligand forming a hydrogen bond with the carboxylate of GLY-753 (Figure 5A) and the remaining two poses displayed less prominent interactions. In all ten poses of $[\mathbf{5}]^{2+}$, the ruthenium atom interacted with the negatively charged carboxylate of the GLU-792-residue (Figure 5B). Two distinct crystal structures, namely PDB 7WC6 and 7WC4, were utilized for the serotonin receptor. In 7WC6, no poses were identified that exhibited any notable interaction with the protein. Conversely, poses obtained after docking to 7WC4 revealed some interactions. Three of the ten poses of $[\mathbf{3}]^{2+}$ displayed no significant interaction, while three other poses exhibited a hydrogen bond interaction of the hydroxyl of the Hmte ligand with the backbone of PHE-234, and four poses established a similar interaction with the carboxylate group of ASP-155. For $[\mathbf{5}]^{2+}$, three poses were located outside the binding pocket, while the remaining seven were situated within the pocket, but lacked coordination interactions with the ruthenium atom. Only a long-range hydrogen bond interaction of 3.5 Å with SER-219 was observed (Figure S4). Those data suggest that $[\mathbf{3}]^{2+}$ might bind at the similar amino acids as serotonin but not as LSD. In contrast to the NMDA and serotonin receptors, the docking procedure of $[\mathbf{3}]^{2+}$ and $[\mathbf{5}]^{2+}$ with receptors CAMK2, CAMK4 and AChE did not result in any pose exhibiting significant interaction with the protein. Overall, these

data pointing to an interaction of $[\mathbf{3}]^{2+}$ and $[\mathbf{5}]^{2+}$ with the NMDA receptors is more likely than binding to serotonin receptors.

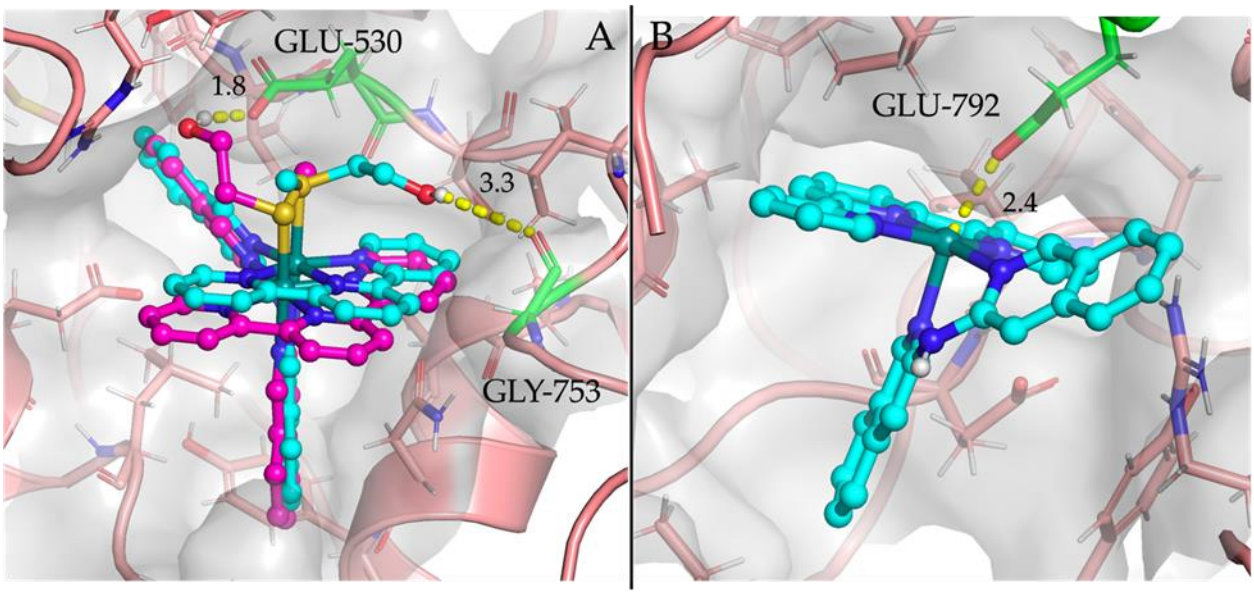

Figure 5. Poses obtained by docking $[\mathbf{3}]^{2+}$ (A) and $[\mathbf{5}]^{2+}$(B) in the pocket of NMDA (PDB: 7EOR). The hydroxyl group of the Hmte ligand of $[\mathbf{3}]^{2+}$ forms a hydrogen bond with the carbonyl of the backbone of GLY-753 (cyan) or the carboxylate of GLU-530 (purple), whereas the ruthenium atom of $[\mathbf{5}]^{2+}$ is coordinated to the negatively charged carboxylate of GLU-792. Distances are in Angstrom. Residues that form an interaction with the compounds are highlighted in green.

For the AMPA receptor, we decided to use three different PDB (4LZ5, 4LZ7, 5YBG) structures that either included the natural inhibitor glutamate, or an allosteric inhibitor. For the PDB file 4LZ7, no interactions with $[\mathbf{3}]^{2+}$ or $[\mathbf{5}]^{2+}$ and the binding pocket were found. Also, for the other two structures we found that $[\mathbf{3}]^{2+}$ did not form a strong coordination bond in a binding pocket. For $[\mathbf{5}]^{2+}$, the ruthenium atom was found to interact with the oxygen of the hydroxyl group of a serine residue within the active site (Figure 5). In PDB 4LZ5 all poses were found to interact with SER-518. The docking procedure of $[\mathbf{5}]^{2+}$ to 5YBG identified two possible sites of interaction, SER-518 and SER-750. The identification of the same interaction over these two different PDB structures highlights the high probability that $[\mathbf{5}]^{2+}$ interacts with a serine residue in the pocket of the AMPA receptor. This docking screening identified three possible calcium transmembrane transporter targets that $[\mathbf{3}]^{2+}$ and $[\mathbf{5}]^{2+}$ may potentially inhibit: NMDA, the serotonin receptor, and the AMPA receptor. There is a notable difference in interaction strength of the obtained poses of $[\mathbf{3}]^{2+}$ and $[\mathbf{5}]^{2+}$, which could potentially explain the observed difference in Ca^{2+} concentration when

the cells were irradiated with light or kept in the dark. Of course, future experimental investigations should confirm these initial computational results.

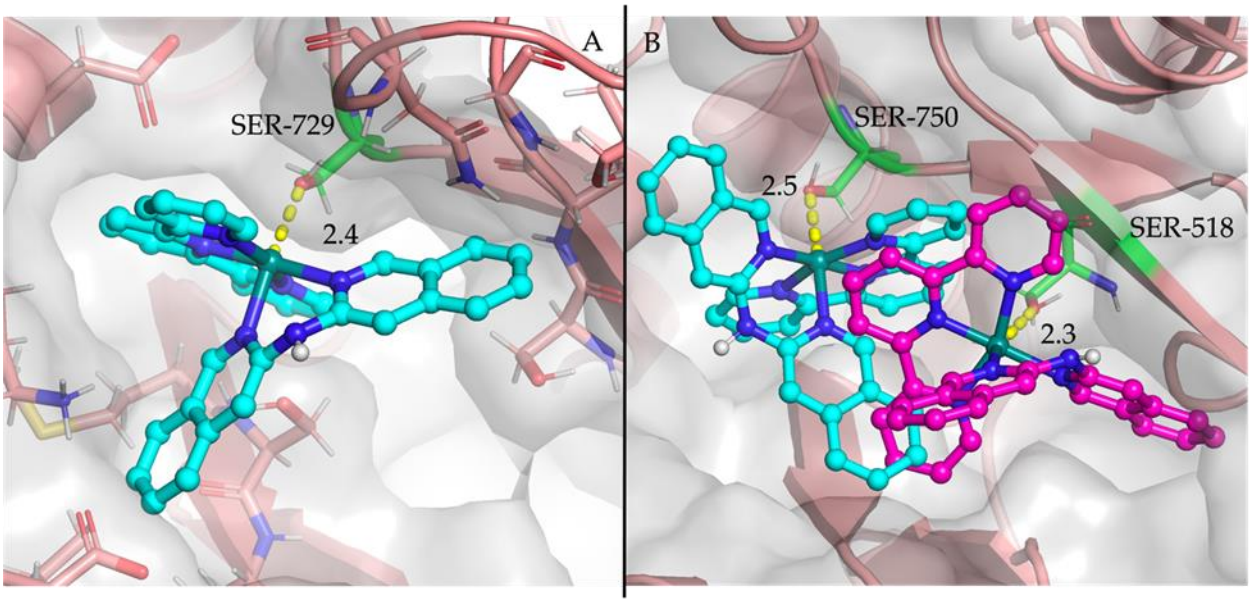

Figure 5. The interaction of $[\mathbf{5}]^{2+}$ and the AMPA receptor according to the MetalDock program. (A) Best pose of $[\mathbf{5}]^{2+}$ in the PDB 4LZ5 structure showing coordination to the SER-729 residue; (B) Two best poses of $[\mathbf{5}]^{2+}$ in the PDB 5YBG structure showing coordination to the SER-750 and SER-518 residues.

General discussion

Albeit ruthenium-based PACT compounds have already demonstrated their anti-cancer effect in a plethora of human cancer cell lines *in vitro* and *in vivo*, many ruthenium polypyridine photocages have been reported to be non-biological active or poorly biologically active and act mostly as carrier for organic inhibitor.[75–77] In addition, the use of ruthenium complexes to treat diseases that affect the brain has been sparsely used to date.[50] In fact, only a few examples of anti-cancer[50] or anti-AD[60–62] ruthenium-based compounds have been published. Despite their effectiveness against cancer or in the re-solubilization of Alzheimer's proteins, little attention has been paid to their effects on the healthy neuronal network.

Within the series of structurally related compounds [**1**]$(PF_6)_2$-[**3**]$(PF_6)_2$, in this new work several trends could be observed, that were highly dependent on the nature of the bidentate ligand. As expected, [**1**]$(PF_6)_2$ was poorly phototoxic due to very low uptake. Surprisingly, changing the bpy ligand by i-biq increased cytotoxicity at least by a 3-fold factor, although uptake did not increase significantly; still, no difference between dark and light cell growth inhibition EC_{50} values were seen for [**2**]$(PF_6)_2$. The best light-activated properties in this series of compounds was observed for [**3**]$(PF_6)_2$, which became 3.5 times more toxic upon green light irradiation compared with dark conditions. Compared with [**2**]$(PF_6)_2$, it was twice less cytotoxic in the dark in spite of the 4 times higher uptake, and twice more cytotoxic after light irradiation. Similarly as in our previous study in A375 and A549 cells,[53] the bidentate ligand regulates the ability of cells to take up these compounds, which increases in the order [**1**]$(PF_6)_2$ < [**2**]$(PF_6)_2$ < [**3**]$(PF_6)_2$. The target of those kind of ruthenium-based compounds is still elusive, however, our observations indicate that [**2**]$(PF_6)_2$ interacts with its biological target independently of the photo-released ligand, whereas [**3**]$(PF_6)_2$ showed more light-induced toxicity.

The antiproliferative effects of [**3**]$(PF_6)_2$ in U-87MG cells made it a good candidate for more detailed neuro-safety investigations. Interestingly, light penetration had a pivotal impact on the growth of neuron-like SH-SY5Y cells as well as on Ru^{2+} uptake and, unexpectedly, on Ca^{2+} cellular penetration. Treatment with our complexes and green light even triggered the proliferation of this cell line, or blocked the antiproliferative effect of green light alone. This strange effect was very similar to that observed, in the same conditions, with Donepezil HCl, which is supposed to

not be photoactive. Several studies pointed out that green light treatment alone can reduce pain[78,79] or cause dendrite elongation, which is connected to increased connectivity and communications between neurons.[66] It is difficult to state if these observations can be attributed to the effects of green light or the drugs itself, as complex [**1**]$(PF_6)_2$ (slightly) reduced the proliferation after irradiation with green light. Noteworthy, high concentrations of Ru within SH-SY5Y cells did not result in enhanced cytotoxicity. The cellular uptake studies revealed that upon light activation there were two to eight times more Ru found within the cells as compared with dark conditions. However, the increased proliferation effect upon green light activation can not be reducible to the amount of Ru^{2+} ions inside the cell. For example, light-activated [**2**]$(PF_6)_2$ showed an increased proliferation upon green light treatment even though five times less Ru^{2+} was recorded in SH-SY5Y cells after light exposure. Consequently, no correlation could be drawn between ruthenium uptake and its inhibitory effects on the cell proliferation in SH-SY5Y cells.

The use of green light also had an effect on the Ca^{2+} uptake on the control cells that are not treated with Ru-based drugs. Under resting conditions, or not excited conditions, the intracellular Ca^{2+} levels in neurons is approximately 0.1-0.5 μM.[67] If those levels are below or above it can cause fatal consequences, also known as excitotoxicity. Excitotoxicity can lead to neuro degeneration, loss of memory and in fatal cases, to stroke. High levels of Ca^{2+} is associated with irreversible cell damage.[63,80] Crucial processes as proliferation and cancer progression are Ca^{2+}-dependent.[81–83]. When we treated the control group with green light, we observed that the intracellular Ca^{2+} amount went up to twice the amount compared when we left the control cells in the dark. As expected, GA treatment in the dark triggered the Ca^{2+} uptake to twice the amount compared with that found in the control cells in the dark. Exceptional results were found by the light treatment of [**3**]$(PF_6)_2$. Almost three times more Ca^{2+} was found when the cells were exposed to the PACT agent and green light. It is noteworthy that such a correlation between Ru^{2+} and Ca^{2+} uptake has not been reported yet. Some ruthenium amine complexes have been reported to inhibit mitochondrial calcium uptake via the blockage of the mitochondrial calcium uniporter.[84,85] To the best of our knowledge, a sharp increase in Ca^{2+} levels following treatment with Ru-based compounds has not been previously observed. The enhanced proliferation rate ([**2**]$(PF_6)_2$) or the reduced anti-proliferative effect ([**1**]$(PF_6)_2$ and [**3**]$(PF_6)_2$), respectively, did not correlate with increased Ca^{2+} levels upon green light activation. Although high Ca^{2+} levels might suggest excitotoxicity, our experimental data do not support the hypothesis that our Ru-based PACT compounds cause cell

death due to elevated Ca^{2+}. In fact, the data suggest the opposite: our compounds might have cell-protective properties.

Of course, the effect of a ruthenium-based PACT compound on calcium cellular uptake opens many questions. Our docking studies suggested various potential mechanisms that may trigger such increase in Ca^{2+} accumulation, namely NMDA, serotonin, and/or AMPA receptor activation. Docking does not model electrons explicitly, and a real covalent interaction cannot be formed in our computational approach. In additional, ruthenium(II) is a soft atom and oxygen-based ligands are often seen as bad ligands for this type of ions. Nonetheless, docking indicates clearly a good fit between the binding pocket and the shape of the molecule, and it is not impossible that a covalent interaction may form between ruthenium in the activated molecule, and the oxygen atom of the serine residue of the AMPA receptor. Such an may explain the sharp increase in Ca^{2+} uptake upon treatment with [**3**]$(PF_6)_2$ and green light irradiation. As note, it is important to distinguish between extrasynaptic and synaptic AMPA receptors as both play a controversial role. Our investigation revealed interaction hits across all docking receptors. However, in contrast to $[\mathbf{3}]^{2+}$ and $[\mathbf{4}]^{2+}$, distinct interactions were observed for NMDA and AMPA receptor, Although, $[\mathbf{3}]^{2+}$ displayed a comparable interaction involving van der Waals and hydrogen bonding near the pocket where Donepezil HCl would interact, $[\mathbf{4}]^{2+}$ primarily demonstrated a single, strong coordination interaction of the ruthenium atom with the GLU-792 residue. Donepezil HCl, on the other hand, showcased a superior fit within the binding pocket (Figure S5), leading to a more potent van der Waals interaction. While this alternative mode of interaction could still yield similar effects, a conclusive understanding would necessitate further exploration of these binding mode through more advanced models such as molecular dynamics.

Nevertheless, AMPA activation is associated with drugs causing seizures.[86] Also the stimulation of extrasynaptic NMDA receptors are reported to contribute to cell death,[87] while evidence suggested that the activation of synaptic NMDA receptors play a role in the longevity and health of cells.[88]

AChE is also a complex receptor. Several studies have demonstrated that AChE activity is associated with cancer cell proliferation,[89–91] that some cancers overexpress the AChE enzyme, resulting in uncontrolled cell growth and drug resistance,[91] but also that apoptotic cells show increased AChE activity.[92] Although the ruthenium complexes tested in this study showed light-

dependent inhibitory effects in a chemical assay using the isolated AChE enzyme, these data have to be considered with care. It is difficult to draw conclusions on the intracellular behavior of drugs from such chemical enzymatic study. For example, Donepezil HCl inhibited AChE activity at nM concentrations in our chemical assay, but in cells it showed no significant effect on cell proliferation, neither in U-87MG nor in SH-SY5Y cells (Table 1&2, Figure S1). In order to investigate if AChE inhibition really plays a role, further investigations are required such as different expression levels of AChE in both cell lines and cell-based AChE inhibition studies.[93]

Conclusion

In this work we have described the cytotoxic effects of different Ru polypyridine complexes in U-87MG glioblastoma cells. While *in vitro* efficacy studies for glioblastoma treatments come with inherent limitations, our findings strongly suggest the potential of ruthenium-based photoactivated chemotherapy (PACT) complexes such as [**3**]$(PF_6)_2$ for further exploration in glioblastoma therapy. Prodrug [**2**]$(PF_6)_2$ bearing the i-biq ligand already reduced proliferation of GBM cells in the dark, but it showed no activation by light, while [**3**]$(PF_6)_2$ had limited growth inhibitory effect in the dark, but was efficiently activated by green light (PI = 3.5). For the first time, we also examined the biological activity of these compounds in neuron-like SH-SY5Y cells as first step towards safety assessment. Our results indicate that these compounds are cytotoxic only at high concentrations in these non-cancerous cells. Notably, [**3**]$(PF_6)_2$ showed a surprising reversal of toxicity upon light irradiation, a phenomenon similarly observed with the cholinesterase inhibitor Donepezil HCl. Importantly, no correlation was found between Ru uptake in SH-SY5Y cells and reduced cell proliferation. However, clear-cut effects of these ruthenium compounds were observed for the first time on calcium cellular uptake. We found a structure-dependent, light-dependent, but uptake-independent increase of Ca^{2+} uptake of cells treated with [**3**]$(PF_6)_2$. Computational docking studies suggested that light-activated [**3**]$^{2+}$ (i.e., [**4**]$^{2+}$) but not [**3**]$^{2+}$ may interact with the NMDA receptor, potentially explaining the inactivation of the Ca^{2+} influx due to the competitive binding with the antagonist ifenprodil. Our docking results also suggest that the AMPA receptors may be activated by [**4**]$^{2+}$, which would explain elevated Ca^{2+} levels. Our cell studies highlighted an intriguing difference between U-87MG and SH-SY5Y cells: upon treatment

with [**3**]$(PF_6)_2$ light activation increases the toxicity in U-87MG cells, while toxicity in SH-SY5Y cells decreased. This differential response emphasizes the need to consider both cancer and neuron-like cellular models when evaluating the safety and efficacy of Ru-based PACT compounds. Overall, our study suggests that Ru-based PACT compounds have promising potential for the treatment of GBM, but that neurotoxicity and excitotoxicity must be investigated more deeply. These considerations have, to our knowledge, not been considered yet, while they should remain central in the design of new Ru PACT compounds for the treatment of glioblastoma to avoid unintended interactions with Ca^{2+} transporters. Overall, modeling these interactions experimentally and using more advanced computational methods will be critical not only to better understand how ruthenium compounds behave in the brain and influence calcium effluxes, but also as essential steps towards more translational approaches for the treatment of brain cancer with PACT.

Experimental Section

General Materials and Methods. Chemical reagents and solvents were purchased from commercial suppliers (Sigma-Aldrich, Fluka, Alfa Aesar and Acros) and were used without further purification. Compounds [**1**]$(PF_6)_2$-[**3**]$(PF_6)_2$ were obtained as described elsewhere.[53] Donezepil HCl was obtained from Sigma-Aldrich (D6821).

General cell culture methods. The glioblastoma cells U-87MG cells were purchased from ATCC (American Type Culture Collection, Manassas, Virginia, US) and the neuroblastoma SH-SY5Y cells were kindly provided from the Department for Molecular physiology, Leiden University, The Netherlands. Cells were grown in DMEM with phenol red (U-87 MG) or DMEM/F12 with phenol red (SH-SY5Y) (Sigma Aldrich), supplemented with L-glutamine (1%), penicillin and streptomycin (0.1%) and fetal calf serum (FCS, 10%) at 37°C in a 5% CO2/95% air atmosphere and fed/passaged twice weekly.

Dulbecco's Modified Eagle Medium (DMEM, without phenol red, without glutamine) and DMEM/F12, Glutamine-S (GM; 200 mM), trichloroacetic acid (TCA), glacial acetic acid, sulforhodamine B (SRB), and tris(hydroxylmethyl)aminomethane (Trisbase) were purchased from

Sigma Aldrich. FCS was purchased from Hyclone. Penicillin and streptomycin were purchased from Duchefa and were diluted to a 100 mg/mL penicillin/streptomycin solution (P/S). Trypsin and OptiMEM (without phenol red) were purchased from Gibco Life Technologies. Trypan blue (0.4% in 0.81% sodium chloride and 0.06% potassium phosphate dibasic solution) was purchased from BioRad. Plastic disposable flasks and 96-well plates for cytotoxicity assays were purchased from Sarstedt (No. 83.3924). Cells were counted by using a BioRad TC20™ automated cell counter with Biorad cell-counting slides (No. 1450015). Cells were inspected with an Olympus IX81 microscope. UV-vis measurements for analysis of 96-well plates were performed with a M1000 Tecan Reader, Tecan Trading AG, Switzerland, plate shaking was performed on GFL 3016 reciprocating horizontal shaker, Gesellschaft für Labortechnik, Germany.

Cytotoxicity in U-87 MG and SH-SY5Y cells. For each photocytotoxicity experiment, two plates were prepared and treated identically.[53,55,77] One to test the cytotoxicity in dark and light. U-87MG and SH-SY5Y cells were seeded at t = 0 h in 96-well plates at a density of 6.000 and 8.000 cells/well (100 µL), respectively in OptiMEM supplemented with 2.5% v/v FCS, 0.1% v/v P/S, and 1.0% v/v GM (hereafter called OptiMEM complete) and incubated for 24 h at 37° ºC and 5.0% CO_2. Only the inner 60 wells were used for seeding, the outer wells were equipped with 100 µL OptiMEM to prevent border effects during irradiation. At t = 24 h, aliquots (100 µL) of six different concentrations (1, 10, 25, 50, 75 and 100 µM) of freshly prepared stock solutions (10 mM) of the compounds in OptiMEM complete were added to the wells in triplicate and incubated for additional 24 h. Sterilized dimethylsulfoxide (DMSO) was used to dissolve the compounds in such amounts that the maximum v/v% of DMSO per well did not exceed 0.5 vol% at the highest compound concentration. At t = 48 h, the plates were irradiated with the cell-irradiation setup[94] (520 nm, 30 min, 25.2 J/cm^2) and the control dark plate was kept in the dark. After irradiation, all plates were further incubated in the dark for another 48 h. The cells were fixated at t=96 h by adding cold TCA (10% w/v; 100 µL) in each well and the plates were stored at 4 ºC for 24 h. The TCA medium mixture was removed from the wells, rinsed with demineralized water (3 X). Afterwards, each well was stained with 100 µL SRB (0.6% w/v in 1% v/v acetic acid) for 30 min shaking with GFL 3016 reciprocating horizontal shaker 0-300 rpm. The SRB solution was removed by washing with acetic acid (1% v/v), and air dried. The SRB dye was solubilized with Tris base (10 mM; 200 µL) overnight, and the absorbance in each well was read at λ = 510 nm using M100 Tecan Reader.

The SRB absorbance data for each compound and concentration was averaged over three identical wells (technical replicates, nt = 3) in Excel and was exported to GraphPad Prism. Relative cell populations were calculated by dividing the average absorbance of the treated wells by the average absorbance of the untreated wells. It was checked that the cell viability of the untreated cells of the samples irradiated were similar (maximum difference of 10%) to the non-irradiated samples to make sure no harm was done by light alone. The resulting dose-response curve for each compound in dark and irradiated conditions was fitted to a non-linear regression function with fixed y maximum (100%) and minimum (0%) (relative cell viability) and a variable Hill slope (Equation 1).

$$Y = 100/ (1+10((\log_{10}EC_{50}-X) \cdot HillSlope)) \quad \text{Equation 1}$$

The data of three independent biological replications was averaged to obtain the final effective concentrations (EC_{50} in µM). Photoindices (PI) were calculated for each compound, by dividing the EC_{50} value obtained in the dark by the EC_{50} value determined under light irradiation.

Cellular uptake studies in U-87MG cells. Materials. 65% Nitric acid (Suprapur, Merck) was used in the sample digestion process, while diluted 1% nitric acid (v/v) was employed as a carrying solution throughout the ICP measurements. For preparation of calibration and internal standards National Institute of Standards and Technology (NIST)-traceable 1000 mg/L elemental standards were used (TraceCERT, Fluka). Approximately 18 MΩ cm^{-1} water (Milli-Q) was employed in all sample preparation and analysis steps.

Instrumentation. Calibration standards were prepared in a Secuflow fume hood (SCALA) to prevent contamination by atmospheric particulates. The standard samples and measurement samples were analyzed for trace elements using the NexION 2000 (PerkinElmer) ICP-MS instrument equipped with a concentric glass nebulizer and Peltier-cooled glass spray chamber. An SC2 DX autosampler (PerkinElmer) was connected to the ICP-MS for sample introduction. Syngistix software for ICP-MS (v.2.5, PerkinElmer) was used for all data recording and processing. Five trace elemental calibration standards for ICP-MS analysis were prepared using NIST-traceable 1000 mg/L Ru standards: 0, 1, 5, 20, and 100 µg/L. Samples were analyzed without dilution in the original delivery containers to minimize the possibility of contamination. Here, 10 µg/L Rh and In were used as internal standards. To check the calibration, samples were analyzed

with a blank measurement and a repeat measurement of one of the calibration standards. For the calibration curve, the accepted correlation coefficient (Cor.Coeff) was to be found higher than 0.999.

Sample preparation. 1 mL of U-87MG cells were seeded in 12-well plates (Greiner, No. 665180; 400.000 cells per well). After 24 h, 10 µM of complex [**1**]$(PF_6)_2$, [**2**]$(PF_6)_2$ and [**3**]$(PF_6)_2$ was added and incubated for 6 or 24 h, respectively. Afterwards cells were trypsined, collected and centrifuged. The resulting cell pellet was dissolved in 1 mL PBS and counted via BioRad TC20™ automated cell counter. Afterwards, the solution was centrifuged and washed again with PBS with subsequent centrifuging. This washing step was repeated twice. The resulting cell pellet was digested in 0.5 mL 65% HNO_3 overnight in a hot oven (90 °C). The solution was diluted with MilliQ water to 10 mL and the Ru content [ppb] was measured by ICP-MS.

Cell Fractioning. Ru content in different compartments were determined via Fraction-Prep Cell Fractionation Kit (Abcam, Cambridge, UK, no 288085). U-87MG cells were seeded in 25 cm^2 in OptiMEM medium (1.5 x 10^6 cells) for 24 h. Then, 10 µM of [**2**]$(PF_6)_2$ and [**3**]$(PF_6)_2$ was added in 3 adjacent wells (technical triplicates). Untreated cells served as control. After 24 h incubation time, the cells were collected, counted and fractioned according to the manufacturer's procedure. The Ru content in the different fractions was analysed via ICP-MS.

Cellular uptake studies in SH-SH5Y cells. 1 mL of SH-SY5Y cells were seeded in 12-well plates (Greiner, No. 665180; 500.000 cells per well). After 24 h, 20 µM of complex [**1**]$(PF_6)_2$ and [**2**]$(PF_6)_2$ and 10 µM of [**3**]$(PF_6)_2$ was added and incubated for 6 h. One plate was exposed to green light (520 nm, 30 min, 25.2 J/cm^2) while the other one was kept in dark. After additional 24 h incubation time, cells were trypsined, collected and centrifuged. The resulting cell pellet was dissolved in 1 mL PBS and counted via BioRad TC20™ automated cell counter. Afterwards, the solution was centrifuged and washed again with PBS with subsequent centrifuging two more times. The resulting cell pellet was digested in 0.5 mL HNO_3 overnight in a hot oven (90ºC). The solution was diluted with MilliQ water to 10 mL and the Ru and Ca content [ppb] was measured via ICP-MS.

Acetylcholine esterase inhibition assay. Acetylcholine esterase inhibition kit was purchased from Abcam, Cambridge, UK, (No. 138871) and was used with some modifications: The obtained

enzyme was first dissolved in 100 µL MilliQ water with 0.1% bovine serum albumin to make a 50 units/mL solution. The solution was further diluted 1:50 in 50 mM Tris Buffer, pH = 8 (10 µL in 490 µL) and then placed in 4.5 mL 50 mM Tris Buffer, pH = 8. The complexes were first dissolved in DMSO to obtain a 10 mM solution and then further diluted in 50 mM Tris Buffer, pH = 8 to obtain 1, 2.5, 5. 7.5, 10 and 15 µM solutions. 50 µL of the enzyme and 50 µL of the complex solution was added in a 96-well plate in triplicates. Untreated enzymes served as negative control, while treatment with Donepezil HCl at the same concentrations (1, 2.5, 5. 7.5, 10 and 15 µM) as the complex solution was used as positive control. The plates were kept for 30 min in the dark or exposed to green light irradiation (520 nm, 30 min, 25.2 J/cm^2). Meanwhile, a 10 mM solution of acetylthiocholine iodide and 10 mM dithionitrobenzoic acid (DTNB) was prepared. After the respective time, in each well 5 µL of the acetylthiocholine iodide and DTNB mixture was added. The absorbance was read at microplate Tecan reader at 410 nm every 5 min for in total 40 min.

Computational studies. Docking studies were performed using MetalDock[74] were done with the AMS 2021 engine[95] at the TZP/PBE0/COSMO level,[96–99] including the Grimme's D3 dispersion corrections with BJ damping.[100] Relativistic effects were scalarly corrected for by ZORA.[101] The box was centered on the molecule bound to the protein in the PDB files and a 30 x 30 x 30 Å box was used. After deleting the atoms of the bound water molecule of [**5**]$^{2+}$, we performed our docking simulations for [**3**]$^{2+}$ and [**5**-H_2O]$^{2+}$, generating in total ten poses. To analyze the docking results we used PyMOL.[102]

ASSOCIATED CONTENT

Supporting Information. Supporting Information including dose-response curves in U-87MG of [**1**]$(PF_6)_2$-[**3**]$(PF_6)_2$ and Donepezil HCl, Tables of the Ru cellular uptake studies in U-87MG cells after 6 and 24 h, cellular fractioning of [**2**]$(PF_6)_2$ and [**3**]$(PF_6)_2$ in U-87MG cells. Ru and Ca uptake of [**1**]$(PF_6)_2$-[**3**]$(PF_6)_2$ in SH-SY5Y cells. Dose-response curves of [**1**]$(PF_6)_2$-[**3**]$(PF_6)_2$ on isolated AChE enzyme. Docking studies of [**3**]$^{2+}$ and [**4**]$^{2+}$ and Donepezil HCl on NMDA receptor, AMPA receptor, and serotonin receptor.

Author information

Corresponding Author

*Sylvestre Bonnet

Present Addresses

†If an author's address is different than the one given in the affiliation line, this information may be included here.

Author Contributions

The manuscript was written through contributions of all authors. All authors have given approval to the final version of the manuscript.

Acknowledgements

Dr. Ludovic Bretin and Dr. Liyan Zhang are kindly acknowledged for fruitful scientific discussions and for suggesting analytical techniques. Dr. Sipeng Zheng is kindly acknowledged for operating the ICP-MS. The Dutch Organization for Scientific Research (NWO) is kindly acknowledged for a VICI grant to S.B.

Abbreviations

5-ALA	5-amino levulinic acid
AChE	acetylcholine esterase
AMPA	glutamatergic α-amino-3-hydroxy-5-methyl-4-isoxazole propionic acid
BBB	blood brain barrier
bpy	2,2'-bipyridine
CAM2K	calcium/calmodulin dependent protein kinase II

CAM4K	calcium/calmodulin dependent protein kinase IV
CI	confidential index
DMEM	Dulbeccos Modified Eagle Medium
DTNB	5,5′-dithiobis-(2-nitrobenzoic acid)
EC_{50}	half maximal effective concentration
FBS	fetal bovine serum
GABA	gamma-aminobutyric acid
GBM	glioblastoma multiforme
Hmte	2-methylthioethanol
IC_{50}	half maximal inhibitory concentration
ICP-MS	inductively coupled plasma- mass spectrometry
i-biq	bisisoquinoline
i-diqa	di(isoquinolin-3-yl)amine
^3MC	triplet metal centered
^3MLCT	metal-to-ligand charge transfer excited state
$^1O_2$	singlet oxygen
PACT	photoactivated chemotherapy
PDT	photodynamic therapy
PI	photo index
PP IX	protoporphyrin IX
ROS	reactive oxygen species
SRB	sulforhodamine B
tpy	2,2';6',2"-terpyridine
TNB	2-nitro-5-thiobenzoic acid

References

(1) Oronsky, B.; Reid, T. R.; Oronsky, A.; Sandhu, N.; Knox, S. J. A Review of Newly Diagnosed Glioblastoma. *Front. Oncol.* **2021**, *10*, 574012. https://doi.org/10.3389/fonc.2020.574012.
(2) Tan, A. C.; Ashley, D. M.; López, G. Y.; Malinzak, M.; Friedman, H. S.; Khasraw, M. Management of Glioblastoma: State of the Art and Future Directions. *CA. Cancer J. Clin.* **2020**, *70* (4), 299–312. https://doi.org/10.3322/caac.21613.
(3) Https://Www.Cancer.Net/Cancer-Types/Brain-Tumor.
(4) Grech, N.; Dalli, T.; Mizzi, S.; Meilak, L.; Calleja, N.; Zrinzo, A. Rising Incidence of Glioblastoma Multiforme in a Well-Defined Population. *Cureus* **2020**. https://doi.org/10.7759/cureus.8195.
(5) Www.Gliocure.Com/En/Patients/Glioblastoma.
(6) Wakimoto, H.; Mohapatra, G.; Kanai, R.; Curry, W. T.; Yip, S.; Nitta, M.; Patel, A. P.; Barnard, Z. R.; Stemmer-Rachamimov, A. O.; Louis, D. N.; Martuza, R. L.; Rabkin, S. D. Maintenance of Primary Tumor Phenotype and Genotype in Glioblastoma Stem Cells. *Neuro-Oncol.* **2012**, *14* (2), 132–144. https://doi.org/10.1093/neuonc/nor195.
(7) Kesarwani, P.; Prabhu, A.; Kant, S.; Chinnaiyan, P. Metabolic Remodeling Contributes towards an Immune-Suppressive Phenotype in Glioblastoma. *Cancer Immunol. Immunother.* **2019**, *68* (7), 1107–1120. https://doi.org/10.1007/s00262-019-02347-3.
(8) Soroceanu, L.; Murase, R.; Limbad, C.; Singer, E.; Allison, J.; Adrados, I.; Kawamura, R.; Pakdel, A.; Fukuyo, Y.; Nguyen, D.; Khan, S.; Arauz, R.; Yount, G. L.; Moore, D. H.; Desprez, P.-Y.; McAllister, S. D. Id-1 Is a Key Transcriptional Regulator of Glioblastoma Aggressiveness and a Novel Therapeutic Target. *Cancer Res.* **2013**, *73* (5), 1559–1569. https://doi.org/10.1158/0008-5472.CAN-12-1943.
(9) Wen, P. Y. Malignant Gliomas in Adults. *N Engl J Med* **2008**, 16.
(10) Ameratunga, M.; Pavlakis, N.; Wheeler, H.; Grant, R.; Simes, J.; Khasraw, M. Anti-Angiogenic Therapy for High-Grade Glioma. *Cochrane Database Syst. Rev.* **2018**, *2018* (11). https://doi.org/10.1002/14651858.CD008218.pub4.
(11) Lee, F. Y. F.; Workman, P.; Roberts, J. T.; Bleehen, N. M. Clinical Pharmacokinetics of Oral CCNU (Lomustine). *Cancer Chemother. Pharmacol.* **1985**, *14* (2), 125–131. https://doi.org/10.1007/BF00434350.
(12) Ewend, M. G.; Brem, S.; Gilbert, M.; Goodkin, R.; Penar, P. L.; Varia, M.; Cush, S.; Carey, L. A. Treatment of Single Brain Metastasis with Resection, Intracavity Carmustine Polymer Wafers, and Radiation Therapy Is Safe and Provides Excellent Local Control. *Clin. Cancer Res.* **2007**, *13* (12), 3637–3641. https://doi.org/10.1158/1078-0432.CCR-06-2095.
(13) Hotchkiss, K. M.; Sampson, J. H. Temozolomide Treatment Outcomes and Immunotherapy Efficacy in Brain Tumor. *J. Neurooncol.* **2021**, *151* (1), 55–62. https://doi.org/10.1007/s11060-020-03598-2.
(14) De Braganca, K. C.; Janjigian, Y. Y.; Azzoli, C. G.; Kris, M. G.; Pietanza, M. C.; Nolan, C. P.; Omuro, A. M.; Holodny, A. I.; Lassman, A. B. Efficacy and Safety of Bevacizumab in Active Brain Metastases from Non-Small Cell Lung Cancer. *J. Neurooncol.* **2010**, *100* (3), 443–447. https://doi.org/10.1007/s11060-010-0200-2.
(15) Roth, P.; Mason, W. P.; Richardson, P. G.; Weller, M. Proteasome Inhibition for the Treatment of Glioblastoma. *Expert Opin. Investig. Drugs* **2020**, *29* (10), 1133–1141. https://doi.org/10.1080/13543784.2020.1803827.

(16) Boccadoro, M.; Morgan, G.; Cavenagh, J. Preclinical Evaluation of the Proteasome Inhibitor Bortezomib in Cancer Therapy. *Cancer Cell Int.* **2005**, *5* (1), 18. https://doi.org/10.1186/1475-2867-5-18.
(17) Abbott, N. J.; Rönnbäck, L.; Hansson, E. Astrocyte–Endothelial Interactions at the Blood–Brain Barrier. *Nat. Rev. Neurosci.* **2006**, *7* (1), 41–53. https://doi.org/10.1038/nrn1824.
(18) Abbott, N. J.; Patabendige, A. A. K.; Dolman, D. E. M.; Yusof, S. R.; Begley, D. J. Structure and Function of the Blood–Brain Barrier. *Neurobiol. Dis.* **2010**, *37* (1), 13–25. https://doi.org/10.1016/j.nbd.2009.07.030.
(19) Aldape, K.; Brindle, K. M.; Chesler, L.; Chopra, R.; Gajjar, A.; Gilbert, M. R.; Gottardo, N.; Gutmann, D. H.; Hargrave, D.; Holland, E. C.; Jones, D. T. W.; Joyce, J. A.; Kearns, P.; Kieran, M. W.; Mellinghoff, I. K.; Merchant, M.; Pfister, S. M.; Pollard, S. M.; Ramaswamy, V.; Rich, J. N.; Robinson, G. W.; Rowitch, D. H.; Sampson, J. H.; Taylor, M. D.; Workman, P.; Gilbertson, R. J. Challenges to Curing Primary Brain Tumours. *Nat. Rev. Clin. Oncol.* **2019**, *16* (8), 509–520. https://doi.org/10.1038/s41571-019-0177-5.
(20) Wu, W.; Klockow, J. L.; Zhang, M.; Lafortune, F.; Chang, E.; Jin, L.; Wu, Y.; Daldrup-Link, H. E. Glioblastoma Multiforme (GBM): An Overview of Current Therapies and Mechanisms of Resistance. *Pharmacol. Res.* **2021**, *171*, 105780. https://doi.org/10.1016/j.phrs.2021.105780.
(21) Diaz, R. J.; Ali, S.; Qadir, M. G.; De La Fuente, M. I.; Ivan, M. E.; Komotar, R. J. The Role of Bevacizumab in the Treatment of Glioblastoma. *J. Neurooncol.* **2017**, *133* (3), 455–467. https://doi.org/10.1007/s11060-017-2477-x.
(22) Brandes, A. A.; Finocchiaro, G.; Zagonel, V.; Reni, M.; Caserta, C.; Fabi, A.; Clavarezza, M.; Maiello, E.; Eoli, M.; Lombardi, G.; Monteforte, M.; Proietti, E.; Agati, R.; Eusebi, V.; Franceschi, E. AVAREG: A Phase II, Randomized, Noncomparative Study of Fotemustine or Bevacizumab for Patients with Recurrent Glioblastoma. *Neuro-Oncol.* **2016**, *18* (9), 1304–1312. https://doi.org/10.1093/neuonc/now035.
(23) Gerber, D. E.; Grossman, S. A.; Zeltzman, M.; Parisi, M. A.; Kleinberg, L. The Impact of Thrombocytopenia from Temozolomide and Radiation in Newly Diagnosed Adults with High-Grade Gliomas1. *Neuro-Oncol.* **2007**, *9* (1), 47–52. https://doi.org/10.1215/15228517-2006-024.
(24) Bock, H. C.; Puchner, M. J. A.; Lohmann, F.; Schütze, M.; Koll, S.; Ketter, R.; Buchalla, R.; Rainov, N.; Kantelhardt, S. R.; Rohde, V.; Giese, A. First-Line Treatment of Malignant Glioma with Carmustine Implants Followed by Concomitant Radiochemotherapy: A Multicenter Experience. *Neurosurg. Rev.* **2010**, *33* (4), 441–449. https://doi.org/10.1007/s10143-010-0280-7.
(25) Shi, H.; Sadler, P. J. How Promising Is Phototherapy for Cancer? *Br. J. Cancer* **2020**, *123* (6), 871–873. https://doi.org/10.1038/s41416-020-0926-3.
(26) Senders, J. T.; Muskens, I. S.; Schnoor, R.; Karhade, A. V.; Cote, D. J.; Smith, T. R.; Broekman, M. L. D. Agents for Fluorescence-Guided Glioma Surgery: A Systematic Review of Preclinical and Clinical Results. *Acta Neurochir. (Wien)* **2017**, *159* (1), 151–167. https://doi.org/10.1007/s00701-016-3028-5.
(27) Schupper, A. J.; Rao, M.; Mohammadi, N.; Baron, R.; Lee, J. Y. K.; Acerbi, F.; Hadjipanayis, C. G. Fluorescence-Guided Surgery: A Review on Timing and Use in Brain Tumor Surgery. *Front. Neurol.* **2021**, *12*, 682151. https://doi.org/10.3389/fneur.2021.682151.
(28) Lakomkin, N.; Hadjipanayis, C. G. Fluorescence-Guided Surgery for High-Grade Gliomas. *J. Surg. Oncol.* **2018**, *118* (2), 356–361. https://doi.org/10.1002/jso.25154.

(29) Ross, J. L.; Cooper, L. A. D.; Kong, J.; Gutman, D.; Williams, M.; Tucker-Burden, C.; McCrary, M. R.; Bouras, A.; Kaluzova, M.; Dunn, W. D.; Duong, D.; Hadjipanayis, C. G.; Brat, D. J. 5-Aminolevulinic Acid Guided Sampling of Glioblastoma Microenvironments Identifies Pro-Survival Signaling at Infiltrative Margins. *Sci. Rep.* **2017**, *7* (1), 15593. https://doi.org/10.1038/s41598-017-15849-w.
(30) Baig Mirza, A.; Christodoulides, I.; Lavrador, J. P.; Giamouriadis, A.; Vastani, A.; Boardman, T.; Ahmed, R.; Norman, I.; Murphy, C.; Devi, S.; Vergani, F.; Gullan, R.; Bhangoo, R.; Ashkan, K. 5-Aminolevulinic Acid-Guided Resection Improves the Overall Survival of Patients with Glioblastoma—a Comparative Cohort Study of 343 Patients. *Neuro-Oncol. Adv.* **2021**, *3* (1), vdab047. https://doi.org/10.1093/noajnl/vdab047.
(31) Stummer, W.; Pichlmeier, U.; Meinel, T.; Wiestler, O. D.; Zanella, F.; Reulen, H.-J. Fluorescence-Guided Surgery with 5-Aminolevulinic Acid for Resection of Malignant Glioma: A Randomised Controlled Multicentre Phase III Trial. *Lancet Oncol.* **2006**, *7* (5), 392–401. https://doi.org/10.1016/S1470-2045(06)70665-9.
(32) Karges, J.; Chao, H.; Gasser, G. Critical Discussion of the Applications of Metal Complexes for 2-Photon Photodynamic Therapy. *JBIC J. Biol. Inorg. Chem.* **2020**, *25* (8), 1035–1050. https://doi.org/10.1007/s00775-020-01829-5.
(33) McFarland, S. A.; Mandel, A.; Dumoulin-White, R.; Gasser, G. Metal-Based Photosensitizers for Photodynamic Therapy: The Future of Multimodal Oncology? *Curr. Opin. Chem. Biol.* **2020**, *56*, 23–27. https://doi.org/10.1016/j.cbpa.2019.10.004.
(34) Johansson, A.; Faber, F.; Kniebühler, G.; Stepp, H.; Sroka, R.; Egensperger, R.; Beyer, W.; Kreth, F.-W. Protoporphyrin IX Fluorescence and Photobleaching During Interstitial Photodynamic Therapy of Malignant Gliomas for Early Treatment Prognosis. *Lasers Surg. Med.* **2013**, *45* (4), 225–234. https://doi.org/10.1002/lsm.22126.
(35) Wu, S. M.; Ren, Q. G.; Zhou, M. O.; Peng, Q.; Chen, J. Y. Protoporphyrin IX Production and Its Photodynamic Effects on Glioma Cells, Neuroblastoma Cells and Normal Cerebellar Granule Cells in Vitro with 5-Aminolevulinic Acid and Its Hexylester. *Cancer Lett.* **2003**, *200* (2), 123–131. https://doi.org/10.1016/S0304-3835(03)00271-4.
(36) Bonnet, S. Why Develop Photoactivated Chemotherapy? *Dalton Trans.* **2018**, *47* (31), 10330–10343. https://doi.org/10.1039/C8DT01585F.
(37) Bonnet, S. Ruthenium-Based Photoactivated Chemotherapy, *J. Am. Chem. Soc.* **2023**, *145* (43), 23397-23415. https://doi.org/10.1021/jacs.3c01135.
(38) Juris, A.; Balzani, V.; Barigelletti, F.; Campagna, S.; Belser, P.; Zelewsky, A. V. COMPLEXES: PHOTOPI3YSICS, ELECl?ROCHEMISTRY, SCENCE. 193.
(39) Laemmel, A.-C.; Collin, J.-P.; Sauvage, J.-P. Efficient and Selective Photochemical Labilization of a Given Bidentate Ligand in Mixed Ruthenium(II) Complexes of the Ru(Phen)2L2+ and Ru(Bipy)2L2+ Family (L = Sterically Hindering Chelate). *Eur. J. Inorg. Chem.* **1999**, *1999* (3), 383–386.
(40) Rafic, E.; Ma, C.; Shih, B. B.; Miller, H.; Yuste, R.; Palomero, T.; Etchenique, R. RuBi-Ruxolitinib: A Photoreleasable Antitumor JAK Inhibitor. *J. Am. Chem. Soc.* **2024**, *146* (19), 13317–13325. https://doi.org/10.1021/jacs.4c01720.
(41) Chen, Y.; Bai, L.; Zhang, P.; Zhao, H.; Zhou, Q. The Development of Ru(II)-Based Photoactivated Chemotherapy Agents. *Molecules* **2021**, *26* (18), 5679. https://doi.org/10.3390/molecules26185679.
(42) Monro, S.; Colón, K. L.; Yin, H.; Roque, J.; Konda, P.; Gujar, S.; Thummel, R. P.; Lilge, L.; Cameron, C. G.; McFarland, S. A. Transition Metal Complexes and Photodynamic Therapy

from a Tumor-Centered Approach: Challenges, Opportunities, and Highlights from the Development of TLD1433. *Chem. Rev.* **2019**, *119* (2), 797–828. https://doi.org/10.1021/acs.chemrev.8b00211.
(43) Havrylyuk, D.; Heidary, D. K.; Nease, L.; Parkin, S.; Glazer, E. C. Photochemical Properties and Structure–Activity Relationships of RuII Complexes with Pyridylbenzazole Ligands as Promising Anticancer Agents. *Eur J Inorg Chem* **2017**, 8.
(44) Howerton, B. S.; Heidary, D. K.; Glazer, E. C. Strained Ruthenium Complexes Are Potent Light-Activated Anticancer Agents. *J. Am. Chem. Soc.* **2012**, *134* (20), 8324–8327. https://doi.org/10.1021/ja3009677.
(45) Busemann, A.; Araman, C.; Flaspohler, I.; Pratesi, A.; Zhou, X.-Q.; van Rixel, V. H. S.; Siegler, M. A.; Messori, L.; van Kasteren, S. I.; Bonnet, S. Alkyne Functionalization of a Photoactivated Ruthenium Polypyridyl Complex for Click-Enabled Serum Albumin Interaction Studies. *Inorg. Chem.* **2020**, *59* (11), 7710–7720. https://doi.org/10.1021/acs.inorgchem.0c00742.
(46) Meijer, M. S.; Natile, M. M.; Bonnet, S. 796 Nm Activation of a Photocleavable Ruthenium(II) Complex Conjugated to an Upconverting Nanoparticle through Two Phosphonate Groups. *Inorg. Chem.* **2020**, *59* (20), 14807–14818. https://doi.org/10.1021/acs.inorgchem.0c00043.
(47) van Rixel, V. H. S.; Ramu, V.; Auyeung, A. B.; Beztsinna, N.; Leger, D. Y.; Lameijer, L. N.; Hilt, S. T.; Le Dévédec, S. E.; Yildiz, T.; Betancourt, T.; Gildner, M. B.; Hudnall, T. W.; Sol, V.; Liagre, B.; Kornienko, A.; Bonnet, S. Photo-Uncaging of a Microtubule-Targeted Rigidin Analogue in Hypoxic Cancer Cells and in a Xenograft Mouse Model. *J. Am. Chem. Soc.* **2019**, *141* (46), 18444–18454. https://doi.org/10.1021/jacs.9b07225.
(48) Zayat, L.; Calero, C.; Alborés, P.; Baraldo, L.; Etchenique, R. A New Strategy for Neurochemical Photodelivery: Metal−Ligand Heterolytic Cleavage. *J. Am. Chem. Soc.* **2003**, *125* (4), 882–883. https://doi.org/10.1021/ja0278943.
(49) Kumar, P.; Mondal, I.; Kulshreshtha, R.; Patra, A. K. Development of Novel Ruthenium(II)–Arene Complexes Displaying Potent Anticancer Effects in Glioblastoma Cells. *Dalton Trans.* **2020**, *49* (38), 13294–13310. https://doi.org/10.1039/D0DT02167A.
(50) Zhang, L.; Wang, P.; Zhou, X.-Q.; Bretin, L.; Zeng, X.; Husiev, Y.; Polanco, E. A.; Zhao, G.; Wijaya, L. S.; Biver, T.; Le Dévédec, S. E.; Sun, W.; Bonnet, S. Cyclic Ruthenium-Peptide Conjugates as Integrin-Targeting Phototherapeutic Prodrugs for the Treatment of Brain Tumors. *J. Am. Chem. Soc.* **2023**, *145* (27), 14963–14980. https://doi.org/10.1021/jacs.3c04855.
(51) Abyar, S.; Huang, L.; Husiev, Y.; Bretin, L.; Chau, B.; Ramu, V.; Wildeman, J. H.; Belfor, K.; Wijaya, L. S.; Van Der Noord, V. E.; Harms, A. C.; Siegler, M. A.; Le Dévédec, S. E.; Bonnet, S. Oxygen-Dependent Interactions between the Ruthenium Cage and the Photoreleased Inhibitor in NAMPT-Targeted Photoactivated Chemotherapy. *J. Med. Chem.* **2024**, acs.jmedchem.4c00589. https://doi.org/10.1021/acs.jmedchem.4c00589.
(52) Lameijer, L. N.; Brevé, T. G.; van Rixel, V. H. S.; Askes, S. H. C.; Siegler, M. A.; Bonnet, S. Effects of the Bidentate Ligand on the Photophysical Properties, Cellular Uptake, and (Photo)Cytotoxicity of Glycoconjugates Based on the $[Ru(Tpy)(NN)(L)]^{2+}$ Scaffold. *Chem. - Eur. J.* **2018**, *24* (11), 2709–2717. https://doi.org/10.1002/chem.201705388.
(53) Busemann, A.; Flaspohler, I.; Zhou, X.-Q.; Schmidt, C.; Goetzfried, S. K.; van Rixel, V. H. S.; Ott, I.; Siegler, M. A.; Bonnet, S. Ruthenium-Based PACT Agents Based on Bisquinoline

Chelates: Synthesis, Photochemistry, and Cytotoxicity. *JBIC J. Biol. Inorg. Chem.* **2021**, *26* (6), 667–674. https://doi.org/10.1007/s00775-021-01882-8.
(54) Orellana, E.; Kasinski, A. Sulforhodamine B (SRB) Assay in Cell Culture to Investigate Cell Proliferation. *BIO-Protoc.* **2016**, *6* (21). https://doi.org/10.21769/BioProtoc.1984.
(55) Vichai, V.; Kirtikara, K. Sulforhodamine B Colorimetric Assay for Cytotoxicity Screening. *Nat. Protoc.* **2006**, *1* (3), 1112–1116. https://doi.org/10.1038/nprot.2006.179.
(56) Kellog, C. K.; Simmons, R. D.; Miller, R. K.; Ison, J. R. Prenatal Diazepam Exposure in Rats: Long-Lasting Functional Changes in the Offspring. *Neurobehav Toxicol Teratol* **1985**, No. 5, 483–488.
(57) Rodier, P. M. Time of Exposure and Time of Testing in Developmental Neurotoxicology. *NeuroToxicology* **1986**, *7* (2), 69–76.
(58) Moser, V. C. Neurobehavioral Screening in Rodents. *Curr. Protoc. Toxicol.* **1999**, *00*, 11.2.1-11.2.16. https://doi.org/10.1002/0471140856.tx1102s06.
(59) Staff, N. R. C. *Environmental Neurotoxicology*; National Academies Press, 1992.
(60) Vyas, N. A.; Bhat, S. S.; Kumbhar, A. S.; Sonawane, U. B.; Jani, V.; Joshi, R. R.; Ramteke, S. N.; Kulkarni, P. P.; Joshi, B. Ruthenium(II) Polypyridyl Complex as Inhibitor of Acetylcholinesterase and Aβ Aggregation. *Eur. J. Med. Chem.* **2014**, *75*, 375–381. https://doi.org/10.1016/j.ejmech.2014.01.052.
(61) Vyas, N. A.; Singh, S. B.; Kumbhar, A. S.; Ranade, D. S.; Walke, G. R.; Kulkarni, P. P.; Jani, V.; Sonavane, U. B.; Joshi, R. R.; Rapole, S. Acetylcholinesterase and Aβ Aggregation Inhibition by Heterometallic Ruthenium(II)–Platinum(II) Polypyridyl Complexes. *Inorg. Chem.* **2018**, *57* (13), 7524–7535. https://doi.org/10.1021/acs.inorgchem.8b00091.
(62) Peng, Y.-B.; Tao, C.; Tan, C.-P.; Zhao, P. Inhibition of Aβ Peptide Aggregation by Ruthenium(II) Polypyridyl Complexes through Copper Chelation. *J. Inorg. Biochem.* **2021**, *224*, 111591. https://doi.org/10.1016/j.jinorgbio.2021.111591.
(63) Ehrich, M.; Wu, X.; Werre, S. R.; Major, M. A.; McCain, W. C.; Reddy, G. Calcium Signaling in Neuronal Cells Exposed to the Munitions Compound Cyclotrimethylenetrinitramine (RDX). *Int. J. Toxicol.* **2009**, *28* (5), 425–435. https://doi.org/10.1177/1091581809340331.
(64) Martin, E.-R.; Gandawijaya, J.; Oguro-Ando, A. A Novel Method for Generating Glutamatergic SH-SY5Y Neuron-like Cells Utilizing B-27 Supplement. *Front. Pharmacol.* **2022**, *13*, 943627. https://doi.org/10.3389/fphar.2022.943627.
(65) Barner, E. L.; Gray, S. L. Donepezil Use in Alzheimer Disease. *Ann. Pharmacother.* **1998**, *32* (1), 70–77.
(66) Alon, N.; Duadi, H.; Cohen, O.; Samet, T.; Zilony, N.; Schori, H.; Shefi, O.; Zalevsky, Z. Promotion of Neural Sprouting Using Low-Level Green Light-Emitting Diode Phototherapy. *J. Biomed. Opt.* **2015**, *20* (2), 020502. https://doi.org/10.1117/1.JBO.20.2.020502.
(67) Kawamoto, E. M.; Vivar, C.; Camandola, S. Physiology and Pathology of Calcium Signaling in the Brain. *Front. Pharmacol.* **2012**, *3*. https://doi.org/10.3389/fphar.2012.00061.
(68) Sushma; Mondal, A. C. Role of GPCR Signaling and Calcium Dysregulation in Alzheimer's Disease. *Mol. Cell. Neurosci.* **2019**, *101*, 103414. https://doi.org/10.1016/j.mcn.2019.103414.
(69) Wang, Y.; Shi, Y.; Wei, H. Calcium Dysregulation in Alzheimer's Disease: A Target for New Drug Development. *J. Alzheimer's Dis. Park.* **2017**, *7* (5). https://doi.org/10.4172/2161-0460.1000374.

(70) Bondy, S. C. Intracellular Calcium and Neurotoxic Events. *Neurotoxicol. Teratol.* **1989**, *11* (6), 527–531. https://doi.org/10.1016/0892-0362(89)90032-9.
(71) Joshi, M.; Joshi, S.; Khambete, M.; Degani, M. Role of Calcium Dysregulation in Alzheimer's Disease and Its Therapeutic Implications. *Chem. Biol. Drug Des.* **2023**, *101* (2), 453–468. https://doi.org/10.1111/cbdd.14175.
(72) Choi, D. W. Excitotoxicity: Still Hammering the Ischemic Brain in 2020. *Front. Neurosci.* **2020**, *14*, 579953. https://doi.org/10.3389/fnins.2020.579953.
(73) Verma, M.; Lizama, B. N.; Chu, C. T. Excitotoxicity, Calcium and Mitochondria: A Triad in Synaptic Neurodegeneration. *Transl. Neurodegener.* **2022**, *11* (1), 3. https://doi.org/10.1186/s40035-021-00278-7.
(74) Hakkennes, M. L. A.; Buda, F.; Bonnet, S. MetalDock: An Open Access Docking Tool for Easy and Reproducible Docking of Metal Complexes. *J. Chem. Inf. Model.* **2023**, acs.jcim.3c01582. https://doi.org/10.1021/acs.jcim.3c01582.
(75) Bretin, L.; Husiev, Y.; Ramu, V.; Zhang, L.; Hakkennes, M.; Abyar, S.; Johns, A. C.; Le Dévédec, S. E.; Betancourt, T.; Kornienko, A.; Bonnet, S. Red-Light Activation of a Microtubule Polymerization Inhibitor via Amide Functionalization of the Ruthenium Photocage. *Angew. Chem.* **2023**, *n/a* (n/a), e202316425. https://doi.org/10.1002/ange.202316425.
(76) van Rixel, V. H. S.; Ramu, V.; Auyeung, A. B.; Beztsinna, N.; Leger, D. Y.; Lameijer, L. N.; Hilt, S. T.; Le Dévédec, S. E.; Yildiz, T.; Betancourt, T.; Gildner, M. B.; Hudnall, T. W.; Sol, V.; Liagre, B.; Kornienko, A.; Bonnet, S. Photo-Uncaging of a Microtubule-Targeted Rigidin Analogue in Hypoxic Cancer Cells and in a Xenograft Mouse Model. *J. Am. Chem. Soc.* **2019**, *141* (46), 18444–18454. https://doi.org/10.1021/jacs.9b07225.
(77) Lameijer, L. N.; Ernst, D.; Hopkins, S. L.; Meijer, M. S.; Askes, S. H. C.; Le Dévédec, S. E.; Bonnet, S. A Red-Light-Activated Ruthenium-Caged NAMPT Inhibitor Remains Phototoxic in Hypoxic Cancer Cells. *Angew. Chem. Int. Ed.* **2017**, *56* (38), 11549–11553. https://doi.org/10.1002/anie.201703890.
(78) Martin, L.; Porreca, F.; Mata, E. I.; Salloum, M.; Goel, V.; Gunnala, P.; Killgore, W. D. S.; Jain, S.; Jones-MacFarland, F. N.; Khanna, R.; Patwardhan, A.; Ibrahim, M. M. Green Light Exposure Improves Pain and Quality of Life in Fibromyalgia Patients: A Preliminary One-Way Crossover Clinical Trial. *Pain Med.* **2021**, *22* (1), 118–130. https://doi.org/10.1093/pm/pnaa329.
(79) Martin, L. F.; Cheng, K.; Washington, S. M.; Denton, M.; Goel, V.; Khandekar, M.; Largent-Milnes, T. M.; Patwardhan, A.; Ibrahim, M. M. Green Light Exposure Elicits Anti-Inflammation, Endogenous Opioid Release and Dampens Synaptic Potentiation to Relieve Post-Surgical Pain. *J. Pain* **2023**, *24* (3), 509–529. https://doi.org/10.1016/j.jpain.2022.10.011.
(80) Bondy, S. C. Intracellular Calcium and Neurotoxic Events. *Neurotoxicol. Teratol.* **1989**, *11* (6), 527–531. https://doi.org/10.1016/0892-0362(89)90032-9.
(81) Maklad, A.; Sharma, A.; Azimi, I. Calcium Signaling in Brain Cancers: Roles and Therapeutic Targeting. *Cancers* **2019**, *11* (2), 145. https://doi.org/10.3390/cancers11020145.
(82) Wojda, U.; Salinska, E.; Kuznicki, J. Calcium Ions in Neuronal Degeneration. *IUBMB Life* **2008**, *60* (9), 575–590. https://doi.org/10.1002/iub.91.
(83) Seif, F. E.; Azar, S.; Barake, M.; Sawaya, R. Hypercalcemia in Glioblastoma Multiforme. *Neuro Endocrinol. Lett.* **2006**, *27* (4), 547–548.

(84) Zazueta, C.; Sosa-Torres, M. E.; Correa, F.; Garza-Ortiz, A. Inhibitory Properties of Ruthenium Amine Complexes on Mitochondrial Calcium Uptake.
(85) Woods, J. J.; Lovett, J.; Lai, B.; Harris, H. H.; Wilson, J. J. Redox Stability Controls the Cellular Uptake and Activity of Ruthenium-Based Inhibitors of the Mitochondrial Calcium Uniporter (MCU). *Angew. Chem. Int. Ed.* **2020**, *59* (16), 6482–6491. https://doi.org/10.1002/anie.202000247.
(86) Rogawski, M. A. AMPA Receptors as a Molecular Target in Epilepsy Therapy. *Acta Neurol. Scand.* **2013**, *127*, 9–18. https://doi.org/10.1111/ane.12099.
(87) Parsons, M. P.; Raymond, L. A. Extrasynaptic NMDA Receptor Involvement in Central Nervous System Disorders. *Neuron* **2014**, *82* (2), 279–293. https://doi.org/10.1016/j.neuron.2014.03.030.
(88) Hardingham, G. E.; Bading, H. The Yin and Yang of NMDA Receptor Signalling. *Trends Neurosci.* **2003**, *26* (2), 81–89. https://doi.org/10.1016/S0166-2236(02)00040-1.
(89) Xu, H.; Shen, Z.; Xiao, J.; Yang, Y.; Huang, W.; Zhou, Z.; Shen, J.; Zhu, Y.; Liu, X.-Y.; Chu, L. Acetylcholinesterase Overexpression Mediated by Oncolytic Adenovirus Exhibited Potent Anti-Tumor Effect. *BMC Cancer* **2014**, *14* (1), 668. https://doi.org/10.1186/1471-2407-14-668.
(90) Pérez-Aguilar, B.; Vidal, C. J.; Palomec, G.; García-Dolores, F.; Gutiérrez-Ruiz, M. C.; Bucio, L.; Gómez-Olivares, J. L.; Gómez-Quiroz, L. E. Acetylcholinesterase Is Associated with a Decrease in Cell Proliferation of Hepatocellular Carcinoma Cells. *Biochim. Biophys. Acta BBA - Mol. Basis Dis.* **2015**, *1852* (7), 1380–1387. https://doi.org/10.1016/j.bbadis.2015.04.003.
(91) Richbart, S. D.; Merritt, J. C.; Nolan, N. A.; Dasgupta, P. Acetylcholinesterase and Human Cancers. *Adv. Cancer Res.* **2021**, *152*, 1–66. https://doi.org/10.1016/bs.acr.2021.05.001.
(92) Knorr, D. Y.; Demirbas, D.; Heinrich, R. Multifaceted Promotion of Apoptosis by Acetylcholinesterase. *Front. Cell Death* **2023**, *2*, 1169966. https://doi.org/10.3389/fceld.2023.1169966.
(93) Li, S.; Li, A. J.; Zhao, J.; Santillo, M. F.; Xia, M. Acetylcholinesterase Inhibition Assays for High-Throughput Screening. In *High-Throughput Screening Assays in Toxicology*; Zhu, H., Xia, M., Eds.; Springer US: New York, NY, 2022; pp 47–58. https://doi.org/10.1007/978-1-0716-2213-1_6.
(94) Hopkins, S. L.; Siewert, B.; Askes, S. H. C.; Veldhuizen, P.; Zwier, R.; Heger, M.; Bonnet, S. An in Vitro Cell Irradiation Protocol for Testing Photopharmaceuticals and the Effect of Blue, Green, and Red Light on Human Cancer Cell Lines. *Photochem. Photobiol. Sci.* **2016**, *15* (5), 644–653. https://doi.org/10.1039/C5PP00424A.
(95) Te Velde, G.; Bickelhaupt, F. M.; Baerends, E. J.; Fonseca Guerra, C.; Van Gisbergen, S. J. A.; Snijders, J. G.; Ziegler, T. Chemistry with ADF. *J. Comput. Chem.* **2001**, *22* (9), 931–967. https://doi.org/10.1002/jcc.1056.
(96) Ernzerhof, M.; Scuseria, G. E. Assessment of the Perdew–Burke–Ernzerhof Exchange-Correlation Functiona. *J Chem Phys* **1999**, *110* (11), 5029–5036. https://doi.org/10.1063/1.478401.
(97) Pye, C. C.; Ziegler, T. An Implementation of the Conductor-like Screening Model of Solvation within the Amsterdam Density Functional Package. *Theor. Chem. Acc. Theory Comput. Model. Theor. Chim. Acta* **1999**, *101* (6), 396–408. https://doi.org/10.1007/s002140050457.

(98) Chong, D. P.; Van Lenthe, E.; Van Gisbergen, S.; Baerends, E. J. Even-Tempered Slater-Type Orbitals Revisited: From Hydrogen to Krypton. *J Comput Chem* **2004**, *25* (8), 1030–1036. https://doi.org/10.1002/jcc.20030.
(99) Van Lenthe, E.; Baerends, E. J. Optimized Slater-Type Basis Sets for the Elements 1–118. *J Comput Chem* **2003**, *24* (9), 1132–1156. https://doi.org/10.1002/jcc.10255.
(100) Grimme, S.; Ehrlich, S.; Goerigk, L. Effect of the Damping Function in Dispersion Corrected Density Functional Theory. *J. Comput. Chem.* **2011**, *32* (7), 1456–1465. https://doi.org/10.1002/jcc.21759.
(101) Van Lenthe, E.; Snijders, J. G.; Baerends, E. J. The Zero-order Regular Approximation for Relativistic Effects: The Effect of Spin–Orbit Coupling in Closed Shell Molecules. *J. Chem. Phys.* **1996**, *105* (15), 6505–6516. https://doi.org/10.1063/1.472460.
(102) Schrödinger, LLC, 2015.